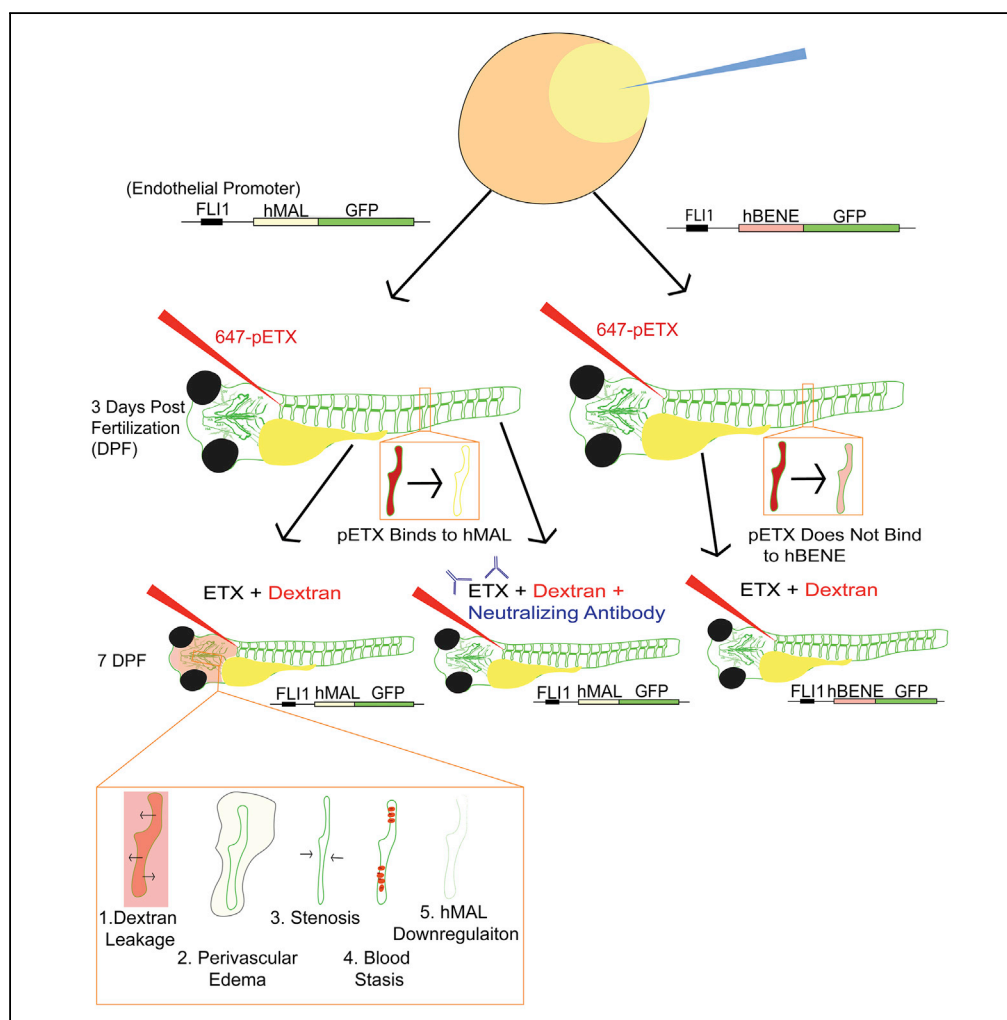


Article

Clostridium perfringens Epsilon Toxin Compromises the Blood-Brain Barrier in a Humanized Zebrafish Model



Drew Adler,
Jennifer R. Linden,
Samantha V.
Shetty, Yinghua
Ma, Monika
Bokori-Brown,
Richard W. Titball,
Timothy Vartanian

tiv2002@med.cornell.edu

HIGHLIGHTS

ProETX binds specifically to hMAL in live humanized zebrafish

hMAL expression in zebrafish confers susceptibility to ETX-mediated BBB breakdown

Live imaging reveals ETX-mediated edema, hMAL downregulation, stenosis, and stasis

Antibody neutralization abrogates ETX-mediated vascular pathology

Adler et al., iScience 15, 39–54
May 31, 2019 © 2019 The Authors.
<https://doi.org/10.1016/j.isci.2019.04.016>



Article

Clostridium perfringens Epsilon Toxin Compromises the Blood-Brain Barrier in a Humanized Zebrafish Model

Drew Adler,^{1,2} Jennifer R. Linden,¹ Samantha V. Shetty,¹ Yinghua Ma,¹ Monika Bokori-Brown,³ Richard W. Titball,³ and Timothy Vartanian^{1,4,*}

SUMMARY

Clostridium perfringens epsilon toxin (ETX) is hypothesized to mediate blood-brain barrier (BBB) permeability by binding to the myelin and lymphocyte protein (MAL) on the luminal surface of endothelial cells (ECs). However, the kinetics of this interaction and a general understanding of ETX's behavior in a live organism have yet to be appreciated. Here we investigate ETX binding and BBB breakdown in living *Danio rerio* (zebrafish). Wild-type zebrafish ECs do not bind ETX. When zebrafish ECs are engineered to express human MAL (hMAL), proETX binding occurs in a time-dependent manner. Injection of activated toxin in hMAL zebrafish initiates BBB leakage, hMAL downregulation, blood vessel stenosis, perivascular edema, and blood stasis. We propose a kinetic model of MAL-dependent ETX binding and neurovascular pathology. By generating a humanized zebrafish BBB model, this study contributes to our understanding of ETX-induced BBB permeability and strengthens the proposal that MAL is the ETX receptor.

INTRODUCTION

The blood-brain barrier (BBB) separates the complex molecular and cellular environment of blood from the refined and acellular environment of cerebrospinal fluid. This highly active functional and physical barrier maintains homeostatic protein and electrolyte concentrations and regulates mononuclear cell count in the human brain by material exclusion, passive transport, and active transport. However, the selectivity of the BBB can be altered dramatically by pathologic processes within the central nervous system (CNS) or factors originating in blood. Furthermore, pharmacologically modulating the BBB to deliver therapeutics into the CNS or repairing the damaged BBB remains major goals in biotechnology. To better understand the molecular mechanisms of a healthy and diseased BBB, we need techniques to visualize and quantify human BBB function in real time.

Clostridium perfringens epsilon toxin (ETX) is a member of the aerolysin family of pore-forming toxins (Cole et al., 2004). One of the most potent bacterial toxins, ETX is considered a potential bioterrorism weapon (Anderson and Bokor, 2012) and is widely known as a causative agent of enterotoxemia and an associated severe multifocal CNS white matter disease in ruminants (Finnie, 2003, 2004; Uzal, 2004; Uzal et al., 2002, 2004). Most of the research on ETX has been conducted in veterinary contexts, whereas a few ETX-mediated diseases have been described in humans (Mantis, 2005). ETX has been proposed as a causative agent in the human demyelinating disease, multiple sclerosis (MS) (Murrell et al., 1986), a hypothesis that has been supported by recent studies (Rumah et al., 2013, 2017; Linden et al., 2015; Wagley et al., 2018). ETX appears to enter the CNS via opening of the BBB (Finnie, 2003). ETX causes a severe reduction in the integrity of BBB vessels (Finnie, 2004; Finnie et al., 2014; Morgan et al., 1975; Nagahama and Sakurai, 1991; Worthington and Mulders, 1975; Zhu et al., 2001), subsequently leading to ETX entry into brain parenchyma (Soler-Jover et al., 2007). However, the mechanism by which it crosses the BBB remains unknown.

ETX's specificity for particular cell types (Bokori-Brown et al., 2011; Dorca-Arevalo et al., 2008; Linden et al., 2015) and its inability to interact with membrane models devoid of protein (Manni et al., 2015) suggests that the toxin acts through a protein receptor. Although the receptor for ETX remains unknown, a few candidate proteins have been identified (Fennessey et al., 2012; Linden et al., 2015; Radaram et al., 2011). The ETX receptor resides on the apical surface (Petit et al., 2003) of detergent-resistant membranes, or lipid rafts, of susceptible cells (Gil et al., 2015; Miyata et al., 2002). ETX binding and cytotoxicity are dependent on

¹Brain and Mind Research Institute, Weill Cornell Medical College of Cornell University, New York, NY 10065, USA

²Department of Neurobiology and Behavior, Cornell University, Ithaca, NY 14850, USA

³Department of Biosciences, University of Exeter, Exeter, Devon EX4 4SB, UK

⁴Lead Contact

*Correspondence: tiv2002@med.cornell.edu

<https://doi.org/10.1016/j.isci.2019.04.016>



the expression of the tetraspanin myelin and lymphocyte protein (MAL) (Rumah et al., 2015). Known to play a role in the formation, stabilization, and maintenance of lipid rafts (Anton et al., 2011; Ramnarayanan and Tuma, 2011; Schaeren-Wiemers et al., 2004; Zhou et al., 2012), MAL is a particularly attractive receptor candidate for ETX as it is expressed in the distal collecting duct of the kidney and myelin of the CNS (Schaeren-Wiemers et al., 1995), two well-defined targets of ETX (Nagahama and Sakurai, 1991; Rumah et al., 2015; Soler-Jover et al., 2007; Tamai et al., 2003). Importantly, studies have also shown MAL to be specifically enriched in mouse brain endothelium (Daneman et al., 2010; Tam et al., 2012; Zhang et al., 2014) and human primary brain endothelial cells (ECs) (Urich et al., 2012). We previously demonstrated that ETX (1) specifically binds to CHO-expressing MAL, (2) specifically kills CHO cells expressing MAL, (3) co-localizes with MAL, (4) does not bind to vasculature or myelin of MAL-deficient mice (MAL^{-/-}), and (5) does not cause *in vitro* demyelination in MAL^{-/-} cerebellar slice culture (Rumah et al., 2015; Linden et al., 2015). Recently, these results have been confirmed, and co-immunoprecipitation experiments exhibiting an association between ETX and human MAL has been achieved, indicating that MAL may be the ETX receptor or at minimum, a crucial component of the ETX pore complex (Blanch et al., 2018).

ETX is released as a 32.9-kDa protoxin (pETX) (Hunter et al., 1992) with approximately 1/1,000th the activity of its activated form (Minami et al., 1997). pETX is subsequently cleaved and activated to more potent forms by extracellular serine proteases (such as trypsin and chymotrypsin) or lambda toxin, a thermolysin-like metalloprotease (Hunter et al., 1992; Minami et al., 1997). pETX and active ETX share essentially identical specificity and affinity for their receptor (Buxton, 1976; Dorca-Arevalo et al., 2008; Gil et al., 2015) as indicated by the protoxin's ability to block active ETX activity and their shared binding to both lipid rafts and identical cell types. Thus pETX is a useful tool for assessing ETX's binding kinetics while maintaining the integrity of the tissue to which it localizes. Unlike pETX, active toxin induces pore formation after binding to a receptor, leading to cell death (Robertson et al., 2011). Pore formation by active ETX is a result of toxin monomer recruitment into homoheptamers on the cell surface, generating a pre-pore complex (Robertson et al., 2011). The pre-pore complex subsequently inserts itself into the lipid bilayer of susceptible cells forming a 0.5- to 1.0-nm pore (Miyata et al., 2001, 2002; Petit et al., 1997). Pore formation in the BBB is thought to initiate an alteration of vascular selectivity and structure (Popoff, 2011). In contrast, protoxin fails to generate oligomers likely due to the steric inhibitory effects of its C terminus in complex formation (Miyata et al., 2001). Studies that have investigated ETX-mediated cellular and molecular pathology have used *in vitro* techniques and ETX-sensitive cell lines or *ex vivo* histology. Our understanding of ETX-mediated BBB permeability has been hindered by the lack of a live, *in vivo* model system allowing for real-time exploration of ETX mechanism and activity in an intact microenvironment.

To study ETX-induced BBB permeability *in vivo*, in real time, we developed an hMAL-expressing zebrafish model system. Zebrafish are particularly ideal for studying *in vivo* BBB integrity and local pathology owing to their small size, low cost, large production of offspring, frequent breeding, and most of all, translucent larval stage, which allows for the visualization of reporter genes in live organisms (Eliceiri et al., 2011; Kim et al., 2017). Transgenic lines have been generated that highlight ECs under the FLI1 enhancer/promoter and allow for the precise study of vasculature (Lawson et al., 2001; Lawson and Weinstein, 2002). Recent studies into zebrafish vascularization have demonstrated the formation of a BBB parallel to that of mammals, with restrictiveness down to 500-Da molecules as early as 3 days post fertilization (DPF) (Fleming et al., 2013; Jeong et al., 2008). In addition, known mammalian BBB tight junction proteins including ZO-1 and claudin-5 have been detected in zebrafish (Jeong et al., 2008; Xie et al., 2010). Utilizing these discoveries and innovations, scientists have used zebrafish to examine the effects of various bacterial and viral infections as well as toxic insults on the integrity of circulatory system and BBB (Bolcome et al., 2008; Ludwig et al., 2011; Mostowy et al., 2013; Takaki et al., 2013). These findings encourage testing ETX-induced barrier dysfunction in this unexploited model organism.

Although zebrafish express MAL, we have previously demonstrated that CHO cells expressing zebrafish MAL (zMAL) do not bind ETX (Rumah et al., 2015). However, this does not exclude the possibility that zebrafish may have another ETX receptor distinct from MAL. In this study, we confirm that zebrafish neurovasculature does not bind ETX and that the introduction of hMAL into EC results in specific, high-affinity binding of protoxin. We further define the specific requirement of MAL for ETX toxicity by showing that BENE, a tetraspanin protein in the MAL family, fails to bind pETX. We provide kinetic evidence for the rapid effect of epsilon toxin on BBB permeability, blood vessel stenosis, focal perivascular edema, and hMAL receptor downregulation in a living organism. Last, we demonstrate that an anti-ETX neutralizing antibody inhibits any evidence of ETX vascular

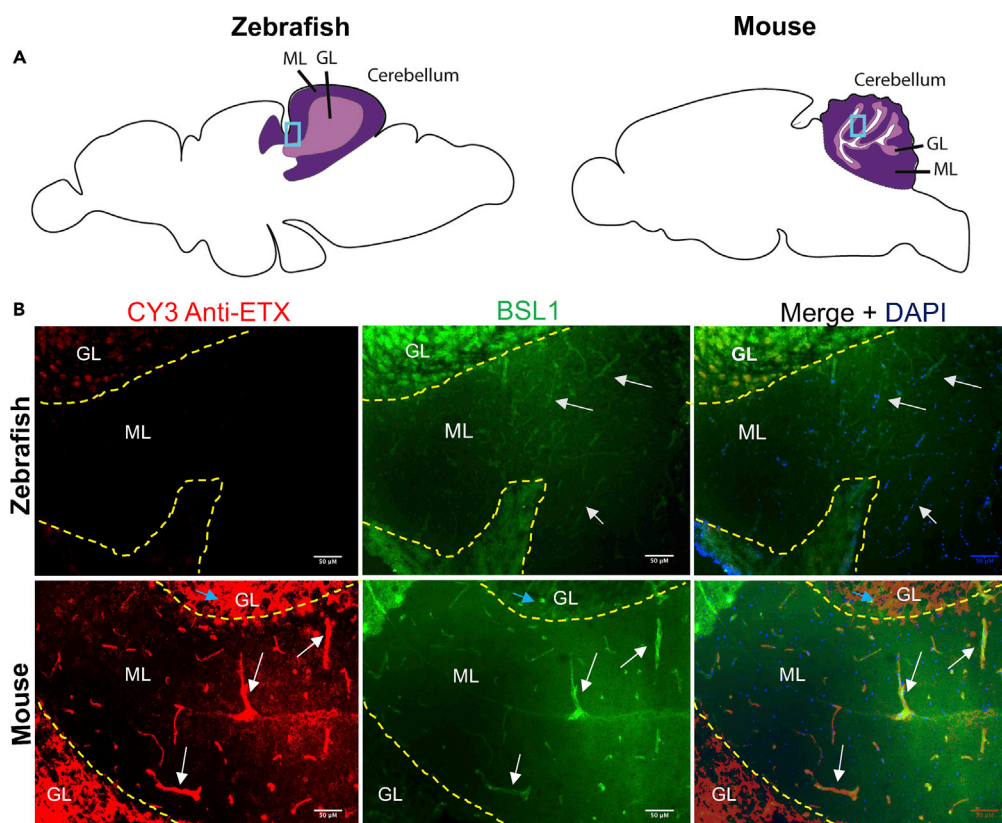


Figure 1. pETX Binds to WT Mouse, but Not WT Zebrafish Neurovasculature

(A) Diagram of mouse and zebrafish sagittal sections with the cerebellum and the region of imaging (blue box) highlighted. (B) Slices from both organisms were probed with pETX and incubated with rabbit anti-ETX primary antibody followed by cy3 anti-rabbit secondary/BSL1. DAPI mounting media in blue highlights nuclei, BSL1 in green highlights vasculature, pETX is in red, "Merge" photo identically stacks all three colored pictures. pETX co-localized with BSL1-highlighted vasculature (white arrows) in all areas of each section of mouse positive controls, as indicated in the yellow vessel in the "Merge" picture, but could not be detected in any zebrafish slice. Toxin also bound strongly to the granular layer of mouse positive controls (blue arrows). Central photos taken at 40 \times magnification with the same exposure time for each condition. ML, molecular layer; GL, granular layer. Scale bars, 50 μ m.

pathology in hMAL-expressing fish. Overall, this gain-of-function study further demonstrates the necessity of MAL for ETX's action, provides indication of ETX-mediated pathology in a humanized model of the BBB, and more generally, elucidates a precise timeline for ETX action in an intact microenvironment.

RESULTS

Wild-Type Zebrafish Do Not Bind ETX in Vasculature

The first step of establishing the suitability of the zebrafish model for ETX toxicity studies was to examine whether the vasculature of wild-type (WT) zebrafish has affinity for ETX. Although it has previously been reported that ETX does not bind the zMAL (Rumah et al., 2015), it is possible that zebrafish express a specific ETX receptor other than MAL. To show that zebrafish lack specific binding sites for ETX, immunohistochemistry was conducted on zebrafish cryosections (Figure 1).

Histological sections of adult (8- to 16-week-old) mouse brain and adult (17 months post fertilization) zebrafish brain were generated. Sagittal sections were incubated with pETX and immunostained for toxin binding using a high-affinity monoclonal antibody against epsilon toxin. Immunohistochemistry revealed that the cerebellar molecular layer of the zebrafish did not bind pETX (Figure 1). In comparison, pETX specifically binds to myelin of the mouse granular layer and localizes to mouse BBB microvessels, highlighted by BSL1 staining (Lonchamp et al., 2010; Linden et al., 2015). Importantly, pETX fails to bind to zebrafish cerebellar vasculature.

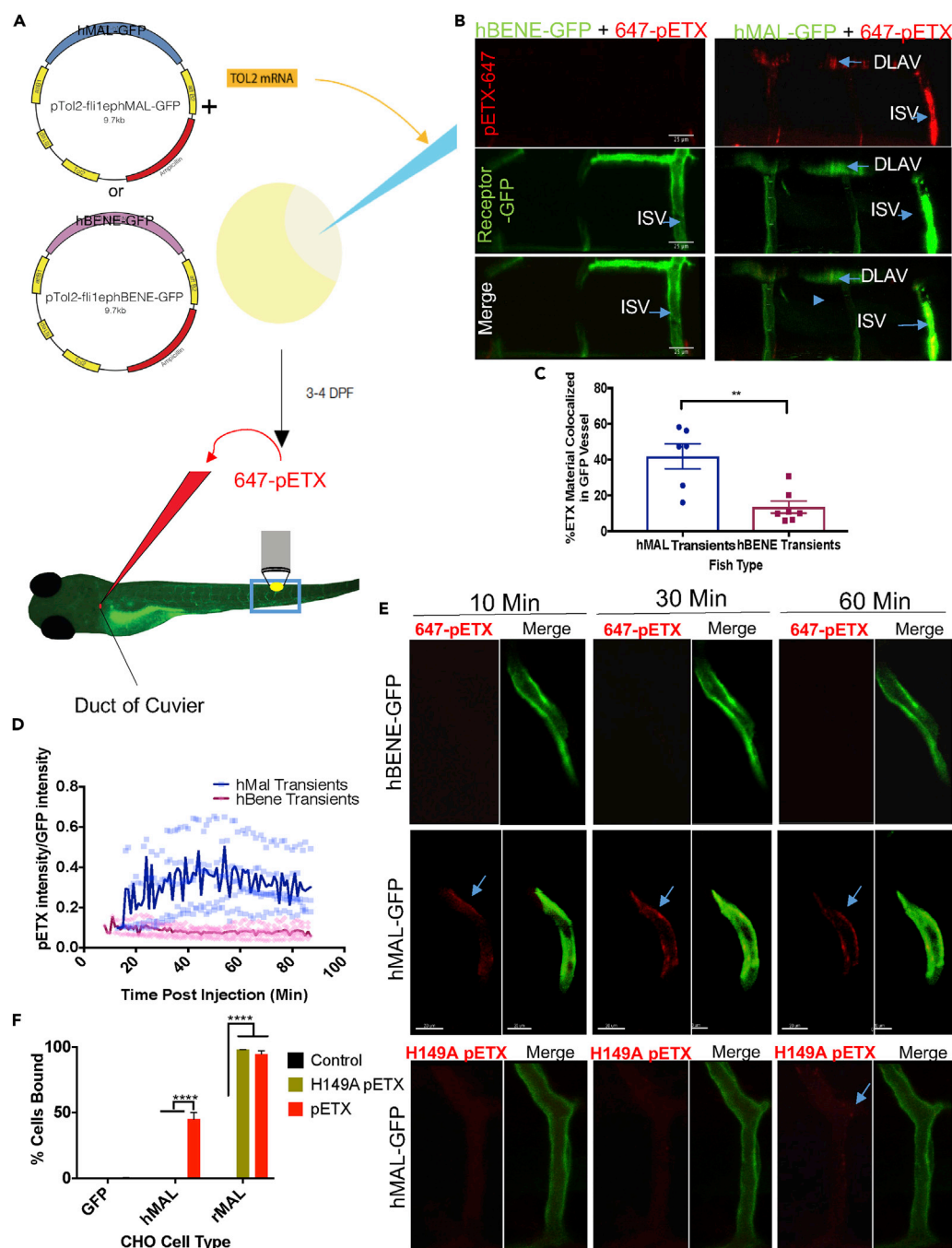


Figure 2. pETX Binds to hMAL-GFP Expressed in Zebrafish ISVs in a Time-Dependent Manner

(A) Schematic depicting zebrafish transformation strategy, toxin injection site, and microscopic focus. Plasmids containing hMAL-GFP or hBENE-GFP were co-injected with tol2 transposase into the cell of 1-cell-stage zebrafish embryos. Positive fish 3-4 days post fertilization (DPF) were injected with Alexa 647-tagged pETX into the duct of Cuvier for systemic infection. The blue box indicates the region imaged in (B).

(B) The 40x confocal z stack images of zebrafish ISVs in hMAL-GFP-expressing fish versus hBENE-GFP-expressing control fish. Scale bar, 25 μ m. ISV, intersegmental blood vessel; DLAV, dorsal longitudinal anastomotic vessel.

(C) Quantitative metric of co-localization, "Percent of ETX Material Co-localized in GFP Vessel," indicates the percentage of pETX voxels co-localized in hMAL-GFP fish ISVs (n = 6 fish) versus hBENE-GFP control ISVs (n = 7 fish) above the automatically set threshold at 1 h post injection. Data are represented as mean \pm SEM. Statistical analysis: unpaired, two-tailed Student's t test (**p < 0.01).

Figure 2. Continued

(D) Equal volumes of GFP along the walls of ISVs were rendered into Imaris surfaces, and sum GFP and 647 intensities within the surface were tracked over the course of ~90 min at 30-s intervals per fish. The ratio of 647-pETX/GFP was plotted over time for hMAL and hBENE transients. Individual ratios of every fish at each time point are represented by opaque circles, and the average ratio at each time point is represented by the darker line.

(E) Snapshot images of 647-pETX or 647-H149A pETX and “merged” images with receptor at three time points post injection. Blue arrow highlights toxin accumulation. Scale bar, 20 μ m.

(F) Flow cytometry analysis of pETX or H149A pETX binding to hMAL, rMAL, or GFP CHO cells.

See also [Videos S1, S2, and S3](#). Statistical analysis: two-way ANOVA with Tukey's test (**** $p < 0.0001$).

Larval Zebrafish Bind ETX Specifically to hMAL-Expressing Blood Vessels

Because zebrafish fail to bind pETX, we used the model organism in gain-of-function experiments to determine if cell-specific expression of hMAL conferred specific ETX binding and if this gene would be sufficient to induce hallmarks of ETX-mediated, vascular pathology. To examine whether ETX binds to hMAL-expressing zebrafish vasculature, zebrafish zygotes were injected with hMAL fused to a GFP reporter (hMAL-GFP) under the FLI1 endothelial promoter/enhancer to generate transient expression ([Figure 2A](#)). Fish that successfully expressed the reporter construct were subsequently injected with Alexa 647-conjugated pETX at 3–4 DPF to look for binding. These preparations were compared with fish injected with plasmids containing a receptor within the same proteolipid family, hBENE-GFP, under the same promoter, to both control for possible non-MAL contingent binding and examine the specificity of the ETX-MAL interaction. Confocal microscopy revealed binding of pETX to vessels expressing hMAL-GFP and undetectable binding, beyond levels of circulating unbound toxin, in hBENE-GFP controls ([Figure 2B](#)).

Analysis of hMAL-GFP- and hBENE-GFP-expressing vessels revealed significant differences in co-localization with Alexa 647-pETX. Co-localization was quantitatively assessed by first setting a GFP threshold to specify EC localization and then determining the percentage of total Alexa 647 pETX signal specifically associated with these GFP voxels ([Figure 2C](#), Student's t test, $p = 0.0028$). To assess the pETX binding kinetics, zebrafish expressing hMAL-GFP or hBENE-GFP were subjected to time-lapse imaging of intersegmental vessels (ISVs) strongly expressing hMAL-GFP or hBENE-GFP. Results indicate that hMAL-GFP binds pETX in a time-dependent manner, as exhibited by Alexa 647 pETX intensity increasing over time within hMAL-GFP vessels, with peak binding occurring 54 min post injection (MPI), whereas pETX-647 intensity decreasing over time within hBENE-GFP vessels and no degree of convincible binding being apparent ([Figures 2D and 2E](#), respectively). Time-lapse videos evidence pETX moving from the lumen to areas of hMAL-GFP in the wall of ISV vessels over time ([Video S1](#)) and not in hBENE-GFP control vessels ([Video S2](#)). To control for non-specific protein-protein interactions, we utilized the pETX H149A mutant, previously shown to have reduced activity to MDCK cells and toxicity in mice ([Oyston et al., 1998](#)) while maintaining structural similarities to the WT toxin ([Bokori-Brown et al., 2013](#)). pETX H149A was fluorescently tagged and injected into fish transiently expressing hMAL-GFP under control of the FLI1 promoter. Two of four fish showed subtle accumulation of fluorescent pETX H149A in hMAL-expressing vessels indicating low affinity to hMAL in a live, *in vivo* context ([Figure 2E](#) and [Video S3](#)). In contrast, by flow cytometry the H149A mutant toxin shows no detectable binding to CHO cells expressing hMAL ([Figure 2F](#)).

Active ETX Causes Leakage of the Blood-Brain Barrier in Fish Expressing hMAL

Having established pETX's specific affinity for hMAL and its binding kinetics in a live *in vivo* context, experiments were then conducted to assess the impact of hMAL on BBB leakage after being challenged with activated toxin ([Figures 3A and 4A](#)). Confocal microscopy revealed progressive leakage of a 2,000-kDa rhodamine dextran dye co-injected with activated ETX from 15 MPI to 2 h post injection (HPI) only in hMAL-expressing fish ($n = 6$, [Figure 3C](#) and [Video S4](#)) and not in controls expressing hBENE ($n = 5$, [Figure 3B](#) and [Video S5](#)). Furthermore, fish expressing hMAL co-injected with H149A mutant ETX also failed to show evidence of vascular leak ($n = 4$, [Figure S3A](#)). In both hBENE and H149A mutant ETX controls, toxin is confined inside blood vessels; this is particularly salient when looking at Imaris surface renderings of the receptor and toxin at 2 HPI ([Figures 3B'](#) and [S3B](#)) as opposed to hMAL fish injected with active toxin ([Figure 3C'](#)). A quantitative assessment of dextran leakage, represented as extracellular/intracellular dextran (“E/I” see [Transparent Methods](#) Equation 1), confirms a significant difference in leakage between hMAL + active ETX conditions and hBENE + active ETX and hMAL + H149A pETX controls at 2 HPI ([Figure 3D](#), two-way ANOVA with Tukey's test, $p \leq 0.0001, 0.0006$) and a significant difference within the hMAL + active ETX group between time point 15 MPI and 2 HPI and 1 HPI and 2 HPI ([Figure 3D](#), two-way ANOVA

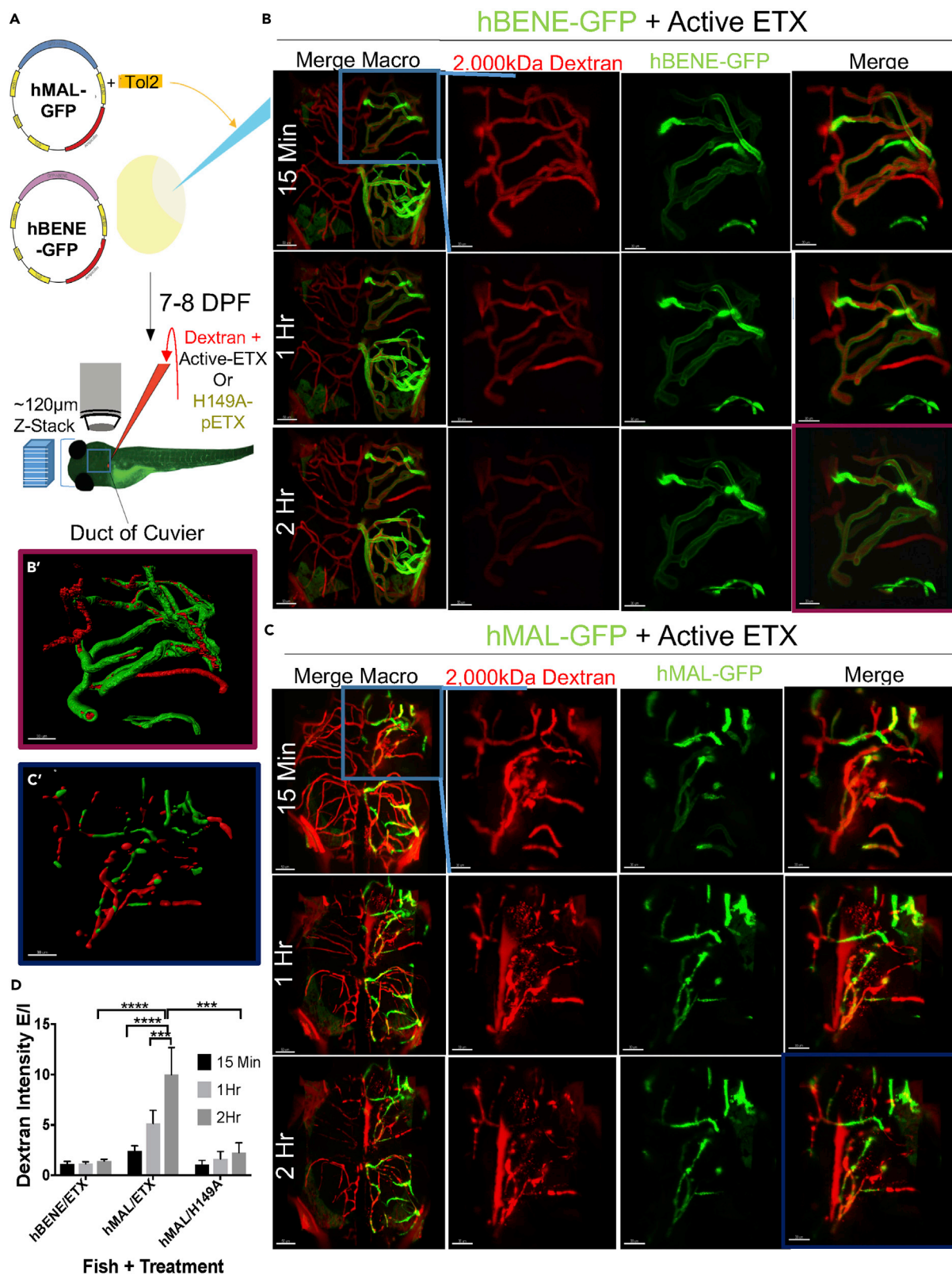


Figure 3. Co-injection of Activated ETX and 2,000-kDa Rhodamine Dextran Reveals Pronounced BBB Leakage in hMAL-Expressing Fish

(A) Schematic depicting experimental procedure.

(B) The 40 \times confocal z stacks of the vasculature in the anterior dorsal quadrant of the brain in a representative hBENE-GFP transiently expressing control zebrafish. hBENE-GFP receptor is in green, the 2,000-kDa rhodamine dextran is in red, “merge” images show both channels, and “Merge Macro” images show full-brain neurovasculature. The blue box in “Merge Macro” highlights the area focused in for the other images; 15 min, 1 h, and 2 h indicate the time z stack imaging commenced after toxin or dextran injection. Scale bar, 50 μ m in “Merge Macro” and 30 μ m in the rest of the images.

(C) Same as (B) but in an hMAL-GFP-expressing fish. (B') Imaris “surface” rendering of hBENE-GFP in green and rhodamine dextran in red used for quantification of GFP sum intensity and total “intravascular” rhodamine sum intensity within the lumen of blood vessels at 2 h post injection. (C') Same as (B') but in hMAL-GFP fish.

(D) Quantification of dextran leakage ascertained by determining extravascular dextran sum intensity divided by intravascular sum intensity (“dextran E/I”) at 15 min, 1 h, and 2 h post injection. Data included from experiment using hBENE-GFP fish injected with active ETX (n = 5), hMal-GFP fish injected with active ETX (n = 6), and hMal-GFP fish injected with mutant control H149A pETX (n = 4).

Data are represented as mean \pm SEM. Statistical analysis: two-way ANOVA with Tukey’s test (***p < 0.001, ****p < 0.0001). See also [Figure S3](#) and [Videos S4](#) and [S5](#).

with Tukey’s test, $p \leq 0.0001, 0.0006$). This finding indicates that a progressive reduction in BBB integrity is robustly apparent only in hMAL-expressing fish treated with active ETX.

Although the FLI1 endothelial promoter/enhancer restricts transgene expression to ECs, the fraction of ECs within an individual fish that expressed the relevant transgene was between 40% and 70%. Incomplete expression within the endothelial lineage often manifested itself as only one-half of the brain expressing the transgene, thus providing us with a novel internal control. Within individual fish an area with high receptor expression was compared with an identical area on the opposite half of the brain with minimal or no observable transgene expression at 2 HPI ([Figures 4B](#) and [4C](#)). Corroborating the finding that hMAL’s expression is a requisite for BBB disruption, at this time point a significant difference in dextran leakage was only seen between these two halves (receptor expressing and receptor absent) in hMAL + active ETX conditions ([Figure 4C](#), two-way ANOVA with Tukey’s test, $p = 0.0008$).

Active ETX Causes Stenosis of BBB Vessels, Perivascular Edema, and Blood Flow Cessation in hMAL Transients

Besides evident leakage, confocal images were examined for the presence of other previously described ETX-induced vascular pathologies and whether hMAL was required for the presence of such phenomena. One previously described finding—vascular lumen compression ([Finnie, 1984a; Sakurai et al., 1983](#))—was evident in the majority of assessed hMAL-expressing vessels ([Figure 5A](#)). Assessment of cerebral central arteries (CCtAs) indicated a progressive decrease in vessel lumen diameter between 15 MPI and 2 HPI in hMAL-expressing vessels challenged with active ETX (n = 6, [Figure 5B](#), two-way ANOVA with Tukey’s test, $p = 0.0193$) but not in hBENE + active ETX (n = 5) or hMAL + H149A pETX controls (n = 3). Significant difference in CCtA lumen diameter started at 1 HPI between hMAL + active ETX and hBENE and H149A controls (two-way ANOVA with Tukey’s Test, $p = 0.0272, 0.0104$). In addition, perivascular edema, a hallmark of both ETX toxicity and MS, was evident in two hMAL-expressing fish ([Figure 5C](#) and [Video S6](#)) and not in controls ([Video S7](#)). In both cases, the locations of edema corresponded directly to regions of dextran leakage and all occurred in vessels with robust receptor expression as early as 15 MPI. Curiously, these areas of acute edema were preferentially seen in vessels traversing through the cerebellum. At 50 MPI, 10-s rapid time-lapse videos of blood flowing through cerebral vessels corroborates this conjecture and indicates the necessity of hMAL, for in hMal-GFP vessels, blood flow appears to completely terminate ([Video S8](#)), whereas in both identical, non-hMAL-expressing vessels within the same fish and within all vessels in control fish, blood flow appears unperturbed ([Videos S9](#) and [S10](#)).

Active ETX Causes hMAL Downregulation

An unforeseen finding revealed in this *in vivo* preparation was the distinct recycling of the hMAL receptor when challenged with active ETX. By 15 MPI, hMAL-GFP expression appears punctate along vessel edges when compared with hBENE-GFP ([Figure 6A](#)). Comparison of hMAL-GFP vessels challenged with active ETX versus H149A mutant pETX reveals that this punctate appearance is mediated by active toxin and is not simply due to a difference between hMAL and hBENE receptor expression, for hMAL vessels challenged with mutant toxin appear indistinguishable from hBENE-expressing vessels challenged with active toxin. Furthermore, images and quantitative analyses reveal that overall receptor protein levels progressively decrease over time in hMAL + active ETX conditions and that there is a significant percent decrease in GFP intensity, and these decreases are seen between both hMAL + active ETX (n = 6) and hBENE + active

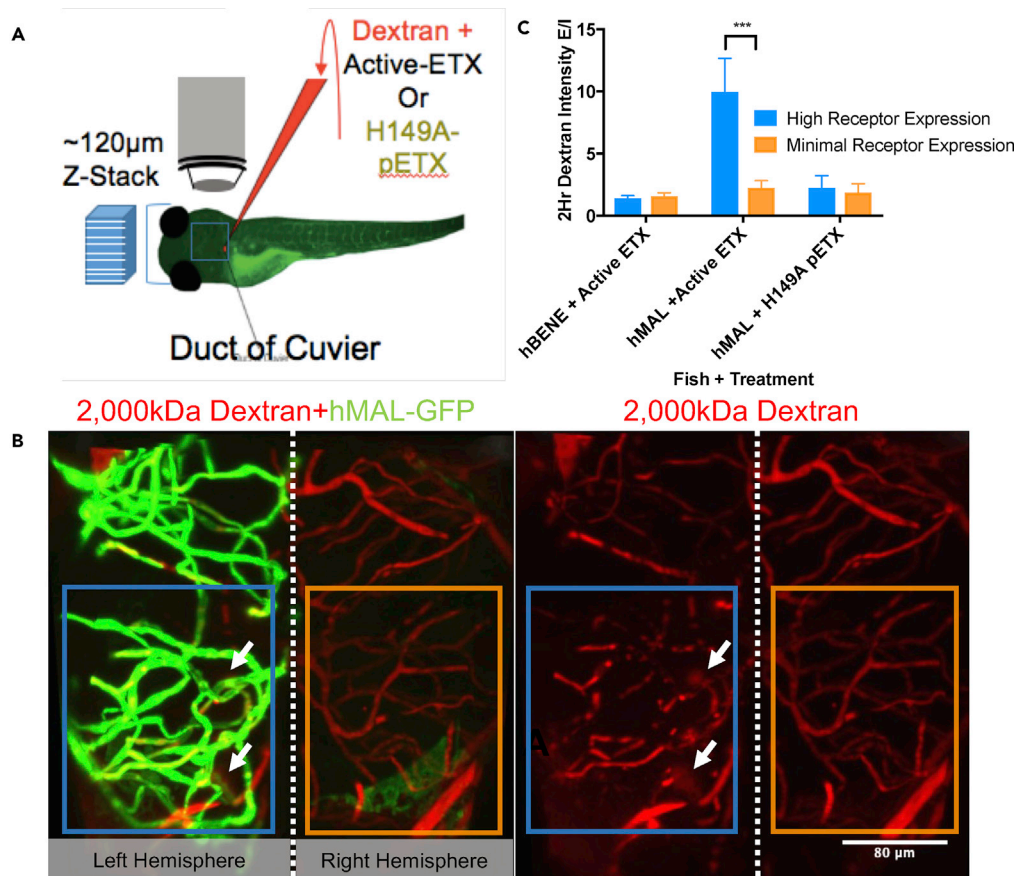


Figure 4. Within Individual hMAL-GFP-Expressing Fish, Dextran Leaks Markedly More in Volumes of the Brain Populated by Receptor-Expressing Vessels than in Areas Without Receptor Expression

(A) Schematic of injection and imaging strategy.

(B) Confocal z stack of a representative fish transiently expressing hMAL-GFP (green) injected with active toxin and 2,000-kDa rhodamine dextran (red) and an adjacent image of just the red dextran channel. Because of the chimeric nature of expression most fish only expressed receptor in discrete parts of the brain, and as depicted, often in half of the brain. White arrows indicate regions of evident leakage. Blue and orange boxes represent the brain quadrants quantified in (C).

(C) Quantification of E/I ratio at 2 HPI between volumes of the brain that have high levels of dextran expression (blue) and those with little dextran expression (orange) for each fish in each condition: hBENE transients injected with active ETX (n = 5/side of brain), hMAL transients injected with active ETX (n = 6/side of brain), hMAL transients injected with H149A mutant pETX (n = 4/side of brain). Significant difference between these two sides of the brain are only seen in the hMAL + active ETX condition (two-way ANOVA with Tukey's test, $p = 0.0008$). Data are represented as mean \pm SEM.

ETX (n = 5) and hMAL + H149A pETX (n = 4) starting at 1 HPI (Figure 6B, two-way ANOVA with Tukey's test, $p = 0.0029, 0.0107$).

Neutralizing Anti-ETX Antibody Inhibits ETX Toxicity

To determine the specificity of ETX cytotoxicity *in vivo*, ETX was pre-incubated with a neutralizing monoclonal antibody, JL008, against ETX before injection into fish expressing hMAL-GFP (n = 4) (Linden et al., 2018). Confocal image analysis of identical experimental parameters revealed dextran well confined within vessels, normal CCtA lumen diameter, and steady blood flow through hMAL-GFP vessels (Video S11). Quantitative analysis confirmed significant difference between neutralized and active ETX E/I at 2 HPI (two-way ANOVA with Tukey's test, $p = 0.0003$) and no significant difference with H149A pETX mutant (Figure 7A). There was also no significant difference in dextran leakage between areas of the brain with hMAL expression and areas without (Figure 7B). CCtA lumen diameter was also significantly different in animals treated with neutralized ETX compared with active ETX (Figure 7C, two-way ANOVA with Tukey's test, $p = 0.0004$). Percent change in hMAL-GFP reduction between 15 MPI and 2 HPI was also significant in animals treated with neutralized ETX compared with active ETX (Figure 7D,

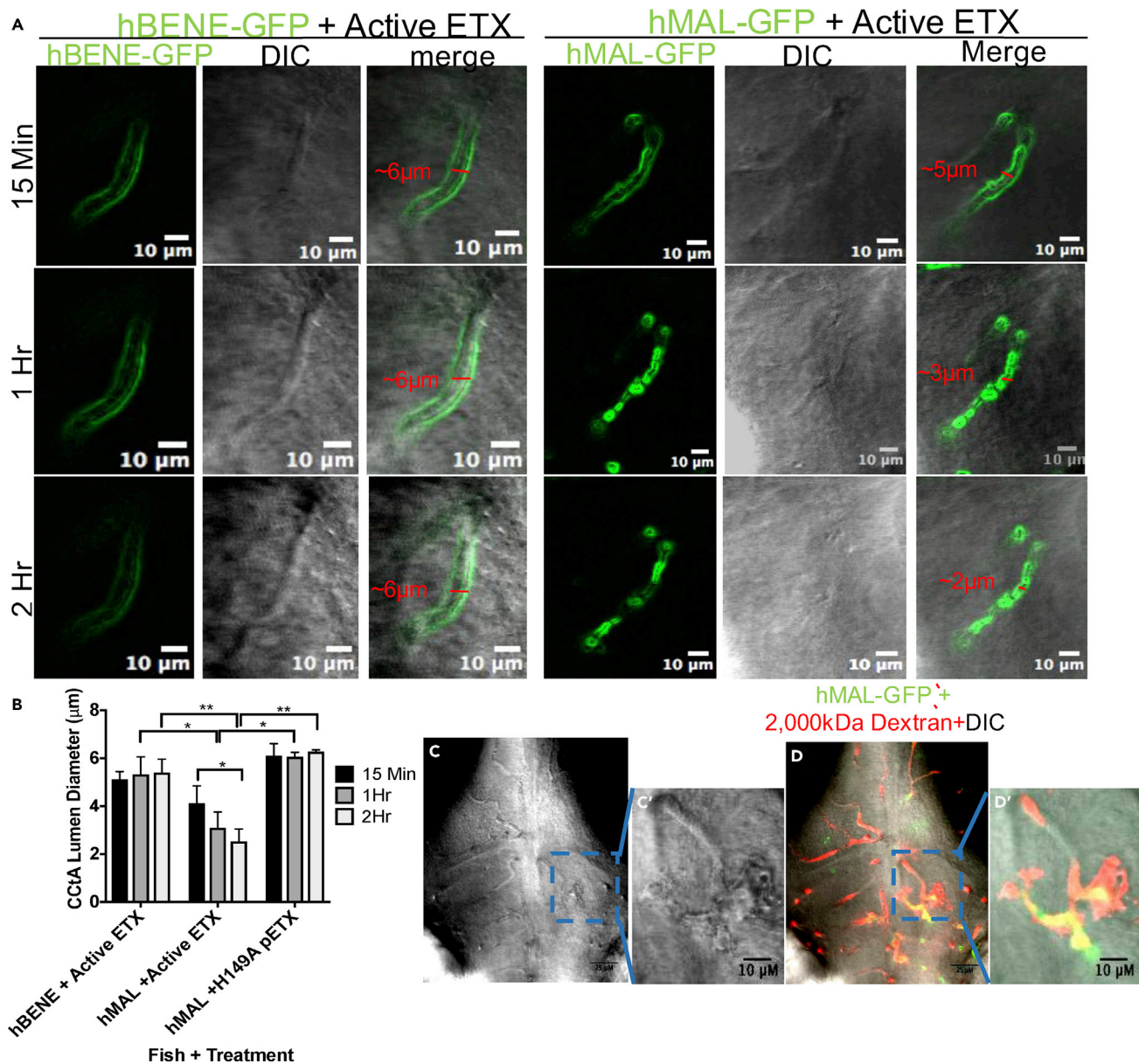


Figure 5. Active ETX Leads to Vessel Stenosis and Perivascular Edema

(A) Zoomed-in confocal images of cerebral central arteries (CCtAs) in hBENE-GFP- and hMAL-GFP-expressing fish 15 min, 1 h, and 2 h post injection with active toxin. Green channels depict receptor expression in these vessels, gray channel depicts differential interference contrast images, “merge” overlays both images. Scale bar, 10 μ m.

(B) Quantitative comparison of CCtA vessel diameter over time for each condition; hMAL CCtA exposed to active ETX are significantly narrower than hBENE CCtAs exposed to ETX or hMAL CCtAs exposed to H149A mutant pETX starting at 1 HPI and showed significant decrease from 15 MPI to 2 HPI (two-way ANOVA with Tukey’s test, * $p < 0.05$, ** $p < 0.01$). Data are represented as mean \pm SEM.

(C) Confocal differential interference contrast macroscopic z-slice of zebrafish brain exhibiting perivascular edema in an hMAL-GFP-expressing fish and (C’) zoomed in single vessel.

(D) Image (C) with merged hMAL-GFP and dextran channels and (D’) merged, zoomed-in single vessel. Scale bar, 25 μ m for full image and 10 μ m for zoomed-in vessel.

See also [Figure S3](#) and [Videos S6, S7, S8, S9, and S10](#).

two-way ANOVA with Tukey’s test, $p = 0.0047$). Thus in all metrics of toxicity, active ETX was effectively neutralized with the neutralizing anti-ETX antibody. Taken together, these data indicate (1) the specificity of ETX-induced pathology and (2) the potential use of this antibody as treatment for ETX-induced disease.

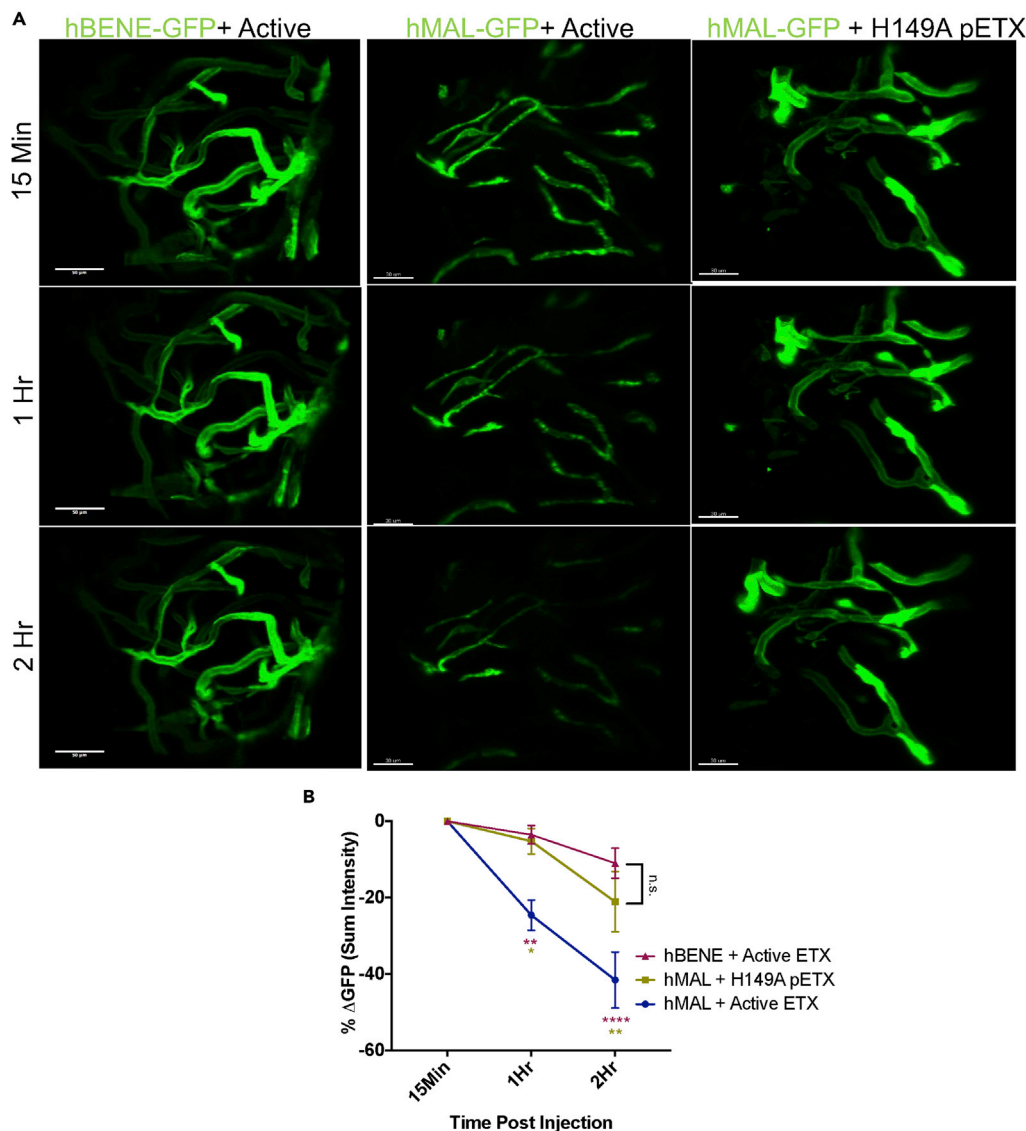


Figure 6. ETX Leads to hMAL Receptor Reduction and Recycling

(A) Representative confocal images of equal volumes of neurovasculature expressing either hBENE-GFP or hMAL-GFP challenged with either active toxin or H149A pETX at 15 MPI, 1 HPI, and 2 HPI. Scale bars, 30 μ m.

(B) Percent change in receptor-GFP sum intensity for each condition using 15 MPI as the starting point. Significant percent change in receptor-GFP intensity reached between hMAL + active ETX and controls starting at 1 HPI (two-way ANOVA with Tukey's test; * $p < 0.05$, ** $p < 0.01$, *** $p < 0.001$, **** $p < 0.0001$). Data are represented as mean \pm SEM.

DISCUSSION

This study, taken as a whole, has provided evidence of real-time ETX binding, receptor downregulation, and BBB disruption via live imaging in a whole animal. Developments in techniques for zebrafish models, including readily available gateway-cloning constructs, reliable injection protocols, and their ease of use in confocal microscopy, have allowed here for precise scrutiny of ETX's action within an intact microenvironment. The organism, when exposed to ETX, gives insights into the sufficiency of the MAL receptor to induce hallmarks of ETX-mediated vascular pathology, for zebrafish only exhibit significant BBB leakage, neurovascular compression, blood-flow cessation, perivascular edema, and receptor downregulation when the hMAL gene is expressed. The presence of transiently expressing mosaic fish, as opposed to stable transgenic fish, further affirms the sufficiency of the receptor, for within individual fish only vascular segments with evident receptor expression demonstrated pathology.

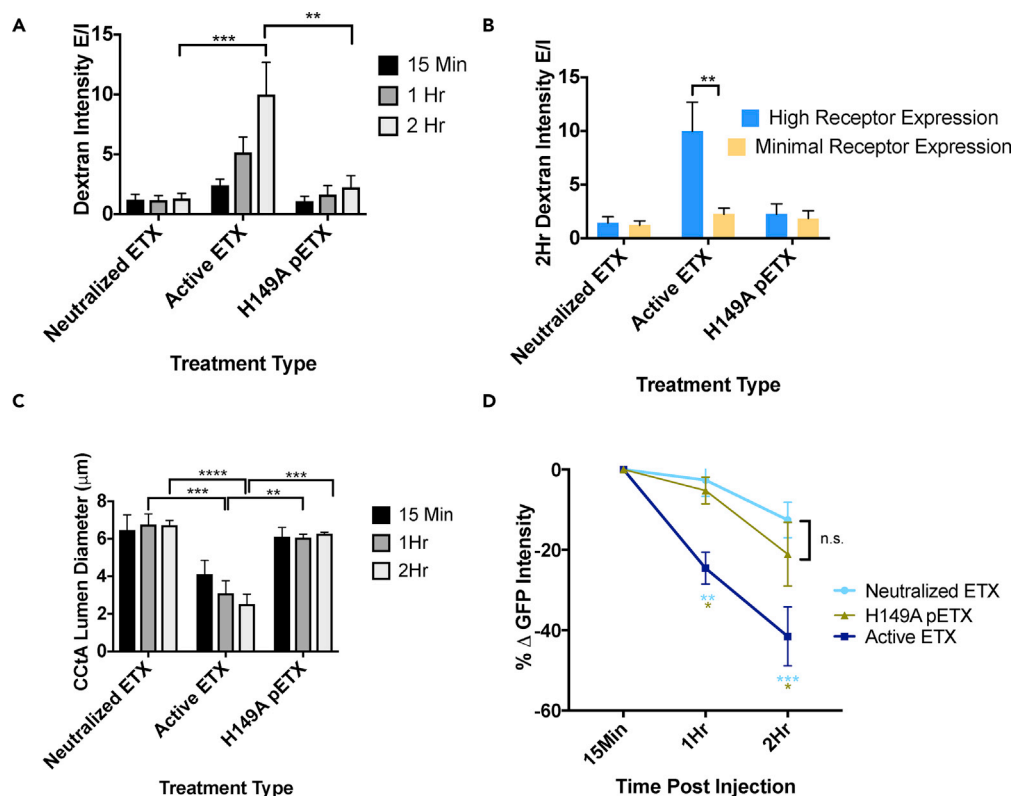


Figure 7. Antibody Neutralization of ETX Eliminates All Metrics of Toxicity

(A and B) (A) Quantitative comparison of dextran leakage (Dextran) in hMAL-GFP-expressing fish injected with neutralized ETX ($n = 4$), active ETX ($n = 6$), or H149A pETX ($n = 4$) from 15 MPI to 2 HPI and (B) dextran leakage between two identical areas of the brain, one with high receptor expression and one with minimal expression.

(C) Quantitative comparison of CCtA lumen diameter in vessels expressing hMAL-GFP treated with the same three preparations.

(D) Quantitative comparison of % change in hMAL-GFP intensity for each treatment using 15 MPI as the baseline.

All statistical analyses using two-way ANOVA with Tukey's test; * $p < 0.05$, ** $p < 0.01$, *** $p < 0.001$, **** $p < 0.0001$). Data are represented as mean \pm SEM. Supporting images in Figures 3 and S2.

Time-lapse imaging allowed for real-time examination of the binding kinetics of pETX to hMAL with peak binding happening approximately 1 h after introduction of toxin into the intravascular space. Peak toxin binding corresponds to the first indication of significant neurovascular changes after ETX treatment. This time point corresponds with the first observations of endothelial damage in mice injected with sublethal doses of activated ETX (Finnie, 1984a) and changes in endothelial barrier antigen after pETX treatment (Zhu et al., 2001)—a further confirmation of the suitability of the zebrafish model for such studies. Certainly, this temporal sequence of vascular pathology would change at different concentrations of toxin; previous studies have shown noticeable leakage of various macromolecules as early as 30 s post intravenous injection using higher, lethal concentrations and tracing much smaller macromolecules (Morgan et al., 1975; Nagahama and Sakurai, 1991; Worthington and Mulders, 1975). Furthermore, although statistical significance was only reached at 1 h, gross imaging suggests leakage and vascular changes as early as 15 MPI. Contrary to previous studies reporting no ETX-induced leakage of large (38.5 kDa) dextrans in *in vitro* polarized MCDK cells (Petit et al., 1997) or BSA using post mortem histopathology (Soler-Jover et al., 2007), this study exhibits drastic leakage of a much larger 2,000-kDa dextran that aggregates at particular hMAL-expressing vessels and diffuses over time. This stark difference in dextran size leakage, between our and previous studies, could be due to developmental and evolutionary differences between the BBB in the zebrafish and rodents. Although the time point chosen (6–7 DPF) is beyond the origin of tight junction protein expression in zebrafish (Xie et al., 2010), and is later than similar toxicological studies (Bolcome et al., 2008; Zhang et al., 2015), the zebrafish BBB does become increasingly selective beyond 6 DPF, as it begins to inhibit larger dextrans (Fleming et al., 2013). Thus an assessment of ETX-induced leakage past 7 DPF is a

possibility for future experimentation, although this later time point requires stable expression of constructs. Leakage of the large dextran could also be due to ectopic overexpression of the hMAL protein, although gross image analysis indicated that the areas with the most abundant hMAL expression were not necessarily the regions that had the most leakage, rather minimal MAL expression was all that was needed for local leakage to be observed. The most likely reason the toxin elicited leakage of such a large tracer was the still relatively high dosage of ETX injected in this study. The ETX dose used in this study most likely led to receptor saturation and maximal pore formation, resulting in massive BBB leakage. The possibility also exists that leakage could be due to cytotoxicity of ECs upon exposure to ETX. Although *in vitro* work indicates that hMAL-expressing CHO cells are highly resistant to death upon exposure to high concentrations of ETX (data not shown), further tests are required to rule this out in an intact microenvironment.

The H149A mutant pETX was also assessed for its relevance as a control for both binding and toxicity experiments. Our studies indicate similar binding affinities of H149A and WT ETX to MDCK cells (data not shown), and previous studies indicate similar structure of the mutant and WT protoxin (Bokori-Brown et al., 2013) while exhibiting reduced toxicity (Oyston et al., 1998). Binding of pETX to hMAL cells and tissue presented here are less conclusive. Although fluorescent co-localization over time in hMAL-expressing fish is certainly reduced when compared with WT pETX, there was clear evidence of a small degree of mutant protoxin accumulation in two of four hMAL ISVs. In contrast, flow cytometry revealed no significant binding of mutant toxin to hMAL, yet significant binding to rMAL. There are many reasons that potentially explain this discrepancy. First, the toxin likely exhibits different binding affinities to different orthologs of MAL. Also, *in vitro* cell-based assays using cell lines may not provide the optimal microenvironment for hMAL-H149ApETX binding. ACHN cells, for instance, show negligible susceptibility to H149A-ETX, even though MDCK cells are susceptible (Bokori-Brown et al., 2013). Possible co-receptors, not expressed in ACHN cells, but expressed *in vivo* in vasculature, may act in concert with MAL to form a suitable H149ApETX-binding site. Alternatively, as the mutant is already recognized to be 67-fold less toxic in mice (Oyston et al., 1998), *in vitro* assays may have been insufficient at detecting mutant protoxin binding to hMAL, for we show that WT protoxin is at baseline bound to less than 50% of hMAL-CHO cells. Our live *in vivo* assay may have been more sensitive and thus revealed modest mutant accumulation. Regardless of the difference between *in vivo* and *in vitro* binding of H149ApETX, this mutant proves a suitable control for toxicity studies, as results here indicated no evidence of H149ApETX-mediated vascular pathology despite binding in two of our four fish.

This study confirms previous findings of ETX-induced BBB vessel stenosis (Finnie, 1984b), perivascular edema (Buxton, 1976; Fernandez-Miyakawa et al., 2008; Freedman et al., 2016; Uzal et al., 2004), and subsequent decreased blood-flow rate (Sakurai et al., 1983). Sakurai et al. (1983) hypothesized that their finding of decreased blood-flow rate in mice injected with active ETX was due to a vascular “pressor” activity of the toxin, for no change in heart rate was observed. Later the same group identified a degree of ETX-mediated aortic constriction, yet affirmed that the most likely cause of ETX-mediated elevated blood pressure was a constriction of resistant arteries (Nagahama and Sakurai, 1992). In our present study, the vessel assessed for changes in diameter (the CCtA) acts as a resistance artery as indicated by its ensheathment by smooth muscle cells (Ando et al., 2016) and its expression of a protein (Yap1) that allows for the change of vessel diameter in response to blood flow (Nakajima et al., 2017). Thus by using *in vivo* imaging, our work confirms the idea that ETX-mediated changes in blood-flow rate are due to its vasoconstrictive capabilities. Furthermore, this study presents real-time imaging of blood flow after ETX injection and indicates a complete halt in blood flow within hMAL-expressing vessels. Such a drastic change in flow suggests that at high doses, ETX-mediated neuropathology may include hypoxia or ischemia. This finding is contrary to an earlier Doppler-based analysis focused on the hippocampus using lower dosages than were used in this study (Miyamoto et al., 1998). Taken together, ETX at low doses appears to lead to leakage of moderate (up to ~38 kDa) tracers (Petit et al., 2003), endothelial blebbing, and perivascular swelling (Finnie, 1984b) while maintaining steady blood flow (Miyamoto et al., 1998). In contrast, ETX at high concentrations, such as the one used in this study, leads to leakage of much larger (as much as 2,000 kDa) dextrans, stark blood vessel compression, and a termination blood flow.

Recently, from a western blot analysis of epsilon-treated human lymphocyte lysates, it has been shown that MAL and epsilon toxin co-immunoprecipitate (Blanch et al., 2018). This suggests that MAL and epsilon toxin exit together in a protein complex and proposes that there may be a direct protein-protein interaction between the two, although this has not yet been proven. Our study corroborates this finding *in vivo*, for we observed co-localization of pETX and hMAL-GFP in live zebrafish. In addition, we detected a

downregulation in hMAL-GFP fluorescence after ETX treatment, raising the possibility that ETX binding to MAL results in internalization and degradation. We also confirmed previous gain-of-function assays demonstrating that MAL is required for both ETX binding and toxicity (Linden et al., 2015). Such downregulation has been reported before *in vitro* using the rodent ortholog of the MAL protein (rMAL) and active toxin (Rumah et al., 2015), although this similar finding with hMAL extends its relevance to human models. Moreover, the exemplification of such a stark phenomenon in an intact microenvironment adds biological significance. Taken together, these data strongly suggest that MAL is the receptor for ETX.

The ETX-specific monoclonal antibody, JL008, completely abrogated all analyzed metrics of ETX-mediated pathology. This both suggests that JL008 is of use as a control for further ETX studies and shortlists it as a potential treatment for ETX intoxication among other tested ETX-neutralizing antibodies (McClain and Cover, 2007; Sakurai et al., 1983). This finding, however, was generated when ETX was incubated for an hour before injection into the live organism. Further tests should be conducted to examine if injection of JL008 after ETX can mitigate the toxin's effects *in vivo* and generate both a time course and a dose course necessary for prevention of ETX-induced pathology. The zebrafish model is already gaining traction as a platform for drug discovery and screening (Kari et al., 2007; MacRae and Peterson, 2015; Parnig et al., 2002; Serbedzija et al., 1999; Taylor et al., 2010). Generation of a transgenic endothelial-specific hMAL-expressing fish line would make this model an ideal candidate for screening anti-ETX treatments via high throughput drug discovery assays.

The use of zebrafish would be ideal to answer a final question regarding the ETX-mediated MS hypothesis: does ETX cause demyelination once in the CNS? Regarding such an assay of demyelination, previous developmental studies have confirmed that zebrafish have robust myelin with oligodendrocytes and Schwann cells, which appear at relatively similar time points as mice, and express many of the same protein markers (Ackerman and Monk, 2016). Recently, the organism has been presented as an option for MS modeling after successful demyelinating results using the canonical lysolecithin (Preston and Macklin, 2015) and experimental allergic encephalomyelitis (EAE) (Kulkarni et al., 2017) MS models. We have previously reported that demyelination occurs in WT mouse models and not in MAL^{-/-} challenged with ETX, yet we have also indicated higher-affinity binding of ETX to rMAL than hMAL and a greater degree of death in rMAL-CHO than in hMAL-CHO cells (Linden et al., 2015). Thus, although it seems reasonable, it is unclear if ETX leads to demyelination in humans. If it does, the toxin concentration necessary to initiate such CNS insults remains unexplored. Humanized models, such as the one presented in this study, can provide these necessary, important insights. The zebrafish is a particularly apt option, for as we have shown here, unlike murine models, it is not normally susceptible to ETX. A particularly compelling follow-up study would be to generate fish that express two reporter-tagged hMAL constructs (using two different reporters) simultaneously in ECs and oligodendrocytes and observe if both BBB penetration and demyelination occur, and if so the kinetics of such pathology. This study has the potential to offer the most comprehensive simulation of ETX-MAL-mediated MS as it may occur in an intact microenvironment.

The body evidence indicating human susceptibility to ETX is limited; however, there are reports of human infection with ETX expressing *C. perfringens* toxinotypes and associated disease. One case report has evidenced a patient with a gangrenous ilium and has isolated ETX secreting *C. perfringens* (type D) (Gleeson-White and Bullen, 1955). In another report ETX was directly isolated from the blood serum of a patient with ankylosing spondylitis (Kohn and Warrack, 1955). In addition, two studies have isolated *C. perfringens* type D from patients with gas gangrene (Morinaga et al., 1965) (Miller et al., 2004). A growing body of evidence has implicated ETX in MS with *C. perfringens* type B (ETX secreting) isolated from a patient with MS and antibodies against the toxin enriched in patient serum (Rumah et al., 2013; Wagley et al., 2018). ETX is known to bind to human renal cell lines (Ivie et al., 2011; Fernandez Miyakawa et al., 2011; Shortt et al., 2000) and cauda equina myelin (Dorca-Arevalo et al., 2008). However, no report has yet shown whether the toxin binds to human BBB. This study's evidence of an association between ETX and hMAL, the interaction's consequential numerous effects on neurovasculature, and MAL's known expression in human BBB (Urich et al., 2012) gives clues as to how ETX might act when circulating through the human bloodstream.

Limitations of the Study

We do not know if there is direct protein-protein interaction between ETX and hMAL or whether there might be other proteins involved in the complex. It is also still unclear whether ETX would still cause the dramatic consequences revealed here at later time points in development as the BBB fully matures or

whether decreased concentrations of ETX would elicit the same findings. Another limitation to the generalizability of this study is the mode of infection (intravenous), which fails to address ETX's transportation from the gut to the bloodstream. We were able to neutralize the effect of the toxin by incubating it, before injection, with a custom monoclonal antibody, yet from a therapeutic standpoint it remains to be seen if the antibody could still mitigate ETX toxicity after the toxin is already in the bloodstream. Finally, it is still unclear what occurs to brain parenchyma after BBB leakage commences.

METHODS

All methods can be found in the accompanying [Transparent Methods supplemental file](#).

SUPPLEMENTAL INFORMATION

Supplemental Information can be found online at <https://doi.org/10.1016/j.isci.2019.04.016>.

ACKNOWLEDGMENTS

We would like to thank the Fetcho lab for providing laboratory space, abundant *Casper zebrafish* fish, consultation, and continual support. In particular J. Fetcho's mentorship and B. Miller's technical expertise were invaluable to the reality of this project. This work was funded in part by the National Institute of Neurological Disorders and Stroke (1R01NS104350, 1R21MS106581) and the Wilma S. and Laurence A. Tisch Foundation.

AUTHOR CONTRIBUTIONS

Conceptualization. D.A., J.R.L., Y.M., and T.V.; Methodology. D.A., J.R.L., and S.V.S.; Analysis. D.A.; Resources, M.B.-B. and R.T.; Supervision, J.R.L. and T.V.; Writing, D.A.

DECLARATION OF INTERESTS

Current US Patent No. 9758573, "Methods to Protect Against and Treat Multiple Sclerosis." Inventors: T.V., Rasheed K. Rumah, J.R.L., Y.M., Vincent A. Fischetti.

Received: September 11, 2018

Revised: December 29, 2018

Accepted: April 8, 2019

Published: May 31, 2019

REFERENCES

- Ackerman, S.D., and Monk, K.R. (2016). The scales and tales of myelination: using zebrafish and mouse to study myelinating glia. *Brain Res.* 1641, 79–91.
- Anderson, P.D., and Bokor, G. (2012). Bioterrorism: pathogens as weapons. *J. Pharm. Pract.* 25, 521–529.
- Ando, K., Fukuhara, S., Izumi, N., Nakajima, H., Fukui, H., Kelsh, R.N., and Mochizuki, N. (2016). Clarification of mural cell coverage of vascular endothelial cells by live imaging of zebrafish. *Development* 143, 1328–1339.
- Anton, O.M., Andres-Delgado, L., Reglero-Real, N., Batista, A., and Alonso, M.A. (2011). MAL protein controls protein sorting at the supramolecular activation cluster of human T lymphocytes. *J. Immunol.* 186, 6345–6356.
- Blanch, M., Dorca-Arevalo, J., Not, A., Cases, M., Gomez de Aranda, I., Martinez Yelamos, A., Martinez Yelamos, S., Solsona, C., and Blasi, J. (2018). The cytotoxicity of Epsilon toxin from *Clostridium perfringens* on lymphocytes is mediated by MAL protein expression. *Mol. Cell Biol.* 38, e00086–18.
- Bokori-Brown, M., Kokkinidou, M.C., Savva, C.G., Fernandes da Costa, S., Naylor, C.E., Cole, A.R., Moss, D.S., Basak, A.K., and Titball, R.W. (2013). *Clostridium perfringens* epsilon toxin H149A mutant as a platform for receptor binding studies. *Protein Sci.* 22, 650–659.
- Bokori-Brown, M., Savva, C.G., Fernandes da Costa, S.P., Naylor, C.E., Basak, A.K., and Titball, R.W. (2011). Molecular basis of toxicity of *Clostridium perfringens* epsilon toxin. *FEBS J.* 278, 4589–4601.
- Bolcome, R.E., 3rd, Sullivan, S.E., Zeller, R., Barker, A.P., Collier, R.J., and Chan, J. (2008). Anthrax lethal toxin induces cell death-independent permeability in zebrafish vasculature. *Proc. Natl. Acad. Sci. U S A* 105, 2439–2444.
- Buxton, D. (1976). Use of horseradish peroxidase to study the antagonism of *Clostridium welchii* (Cl. perfringens) type D epsilon toxin in mice by the formalized epsilon prototoxin. *J. Comp. Pathol.* 86, 67–72.
- Cole, A.R., Gibert, M., Popoff, M., Moss, D.S., Titball, R.W., and Basak, A.K. (2004). *Clostridium perfringens* epsilon-toxin shows structural similarity to the pore-forming toxin aerolysin. *Nat. Struct. Mol. Biol.* 11, 797–798.
- Daneman, R., Zhou, L., Agalliu, D., Cahoy, J.D., Kaushal, A., and Barres, B.A. (2010). The mouse blood-brain barrier transcriptome: a new resource for understanding the development and function of brain endothelial cells. *PLoS One* 5, e13741.
- Dorca-Arevalo, J., Soler-Jover, A., Gibert, M., Popoff, M.R., Martin-Satue, M., and Blasi, J. (2008). Binding of epsilon-toxin from *Clostridium perfringens* in the nervous system. *Vet. Microbiol.* 131, 14–25.
- Eliceiri, B.P., Gonzalez, A.M., and Baird, A. (2011). Zebrafish model of the blood-brain barrier: morphological and permeability studies. *Methods Mol. Biol.* 686, 371–378.
- Fennessey, C.M., Sheng, J., Rubin, D.H., and McClain, M.S. (2012). Oligomerization of *Clostridium perfringens* epsilon toxin is dependent upon caveolins 1 and 2. *PLoS One* 7, e46866.

- Fernandez Miyakawa, M.E., Zabal, O., and Silberstein, C. (2011). Clostridium perfringens epsilon toxin is cytotoxic for human renal tubular epithelial cells. *Hum. Exp. Toxicol.* **30**, 275–282.
- Fernandez-Miyakawa, M.E., Jost, B.H., Billington, S.J., and Uzal, F.A. (2008). Lethal effects of Clostridium perfringens epsilon toxin are potentiated by alpha and perfringolysin-O toxins in a mouse model. *Vet. Microbiol.* **127**, 379–385.
- Finnie, J.W. (1984a). Histopathological changes in the brain of mice given Clostridium perfringens type D epsilon toxin. *J. Comp. Pathol.* **94**, 363–370.
- Finnie, J.W. (1984b). Ultrastructural changes in the brain of mice given Clostridium perfringens type D epsilon toxin. *J. Comp. Pathol.* **94**, 445–452.
- Finnie, J.W. (2003). Pathogenesis of brain damage produced in sheep by Clostridium perfringens type D epsilon toxin: a review. *Aust. Vet. J.* **81**, 219–221.
- Finnie, J.W. (2004). Neurological disorders produced by Clostridium perfringens type D epsilon toxin. *Anaerobe* **10**, 145–150.
- Finnie, J.W., Manavis, J., Casson, R.J., and Chidlow, G. (2014). Retinal microvascular damage and vasogenic edema produced by Clostridium perfringens type D epsilon toxin in rats. *J. Vet. Diagn. Invest.* **26**, 470–472.
- Fleming, A., Diekmann, H., and Goldsmith, P. (2013). Functional characterisation of the maturation of the blood-brain barrier in larval zebrafish. *PLoS One* **8**, e77548.
- Freedman, J.C., McClane, B.A., and Uzal, F.A. (2016). New insights into Clostridium perfringens epsilon toxin activation and action on the brain during enterotoxemia. *Anaerobe* **41**, 27–31.
- Gil, C., Dorca-Arevalo, J., and Blasi, J. (2015). Clostridium perfringens epsilon toxin binds to membrane lipids and its cytotoxic action depends on sulfatide. *PLoS One* **10**, e0140321.
- Gleeson-White, M.H., and Bullen, J.J. (1955). Clostridium welchii epsilon toxin in the intestinal contents of man. *Lancet* **268**, 384–385.
- Hunter, S.E., Clarke, I.N., Kelly, D.C., and Titball, R.W. (1992). Cloning and nucleotide sequencing of the Clostridium perfringens epsilon-toxin gene and its expression in Escherichia coli. *Infect Immun.* **60**, 102–110.
- Ivie, S.E., Fennessey, C.M., Sheng, J., Rubin, D.H., and McClain, M.S. (2011). Gene-trap mutagenesis identifies mammalian genes contributing to intoxication by Clostridium perfringens epsilon-toxin. *PLoS One* **6**, e17787.
- Jeong, J.Y., Kwon, H.B., Ahn, J.C., Kang, D., Kwon, S.H., Park, J.A., and Kim, K.W. (2008). Functional and developmental analysis of the blood-brain barrier in zebrafish. *Brain Res. Bull.* **75**, 619–628.
- Kari, G., Rodeck, U., and Dicker, A.P. (2007). Zebrafish: an emerging model system for human disease and drug discovery. *Clin. Pharmacol. Ther.* **82**, 70–80.
- Kim, S.S., Im, S.H., Yang, J.Y., Lee, Y.R., Kim, G.R., Chae, J.S., Shin, D.S., Song, J.S., Ahn, S., Lee, B.H., et al. (2017). Zebrafish as a screening model for testing the permeability of blood-brain barrier to small molecules. *Zebrafish* **14**, 322–330.
- Kohn, J., and Warrack, G.H. (1955). Recovery of Clostridium welchii type D from man. *Lancet* **268**, 385.
- Kulkarni, P., Yellanki, S., Medishetti, R., Sriram, D., Saxena, U., and Yogeeswari, P. (2017). Novel Zebrafish EAE model: a quick in vivo screen for multiple sclerosis. *Mult. Scler. Relat. Disord.* **11**, 32–39.
- Lawson, N.D., Scheer, N., Pham, V.N., Kim, C.H., Chitnis, A.B., Campos-Ortega, J.A., and Weinstein, B.M. (2001). Notch signaling is required for arterial-venous differentiation during embryonic vascular development. *Development* **128**, 3675–3683.
- Lawson, N.D., and Weinstein, B.M. (2002). In vivo imaging of embryonic vascular development using transgenic zebrafish. *Dev. Biol.* **248**, 307–318.
- Linden, J.R., Ma, Y., Zhao, B., Harris, J.M., Rumah, K.R., Schaeren-Wiemers, N., and Vartanian, T. (2015). Clostridium perfringens epsilon toxin causes selective death of mature oligodendrocytes and central nervous system demyelination. *MBio* **6**, e02513.
- Linden, J.R., Telesford, K., Shetty, S., Winokour, P., Haigh, S., Cahir-McFarland, E., Antognetti, G., Datta, A., Wang, T., Meier, W., et al. (2018). A novel panel of rabbit monoclonal antibodies and their diverse applications including inhibition of Clostridium perfringens epsilon toxin oligomerization. *Antibodies* **7** (4), 37.
- Lonchamp, E., Dupont, J.L., Wioland, L., Courjaret, R., Mbebi-Liegeois, C., Jover, E., Doussau, F., Popoff, M.R., Bossu, J.L., de Barry, J., et al. (2010). Clostridium perfringens epsilon toxin targets granule cells in the mouse cerebellum and stimulates glutamate release. *PLoS One* **5**, e13046.
- Ludwig, M., Palha, N., Torhy, C., Briolat, V., Colucci-Guyon, E., Bremont, M., Herbomel, P., Boudinot, P., and Levraud, J.P. (2011). Whole-body analysis of a viral infection: vascular endothelium is a primary target of infectious hematopoietic necrosis virus in zebrafish larvae. *PLoS Pathog.* **7**, e1001269.
- MacRae, C.A., and Peterson, R.T. (2015). Zebrafish as tools for drug discovery. *Nat. Rev. Drug Discov.* **14**, 721–731.
- Manni, M.M., Sot, J., and Goni, F.M. (2015). Interaction of Clostridium perfringens epsilon-toxin with biological and model membranes: a putative protein receptor in cells. *Biochim. Biophys. Acta* **1848**, 797–804.
- Mantis, N.J. (2005). Vaccines against the category B toxins: Staphylococcal enterotoxin B, epsilon toxin and ricin. *Adv. Drug Deliv. Rev.* **57**, 1424–1439.
- McClain, M.S., and Cover, T.L. (2007). Functional analysis of neutralizing antibodies against Clostridium perfringens epsilon-toxin. *Infect. Immun.* **75**, 1785–1793.
- Miller, C., Florman, S., Kim-Schluger, L., Lento, P., De La Garza, J., Wu, J., Xie, B., Zhang, W., Bottone, E., Zhang, D., et al. (2004). Fulminant and fatal gas gangrene of the stomach in a healthy live liver donor. *Liver Transpl.* **10**, 1315–1319.
- Minami, J., Katayama, S., Matsushita, O., Matsushita, C., and Okabe, A. (1997). Lambdotoxin of Clostridium perfringens activates the precursor of epsilon-toxin by releasing its N- and C-terminal peptides. *Microbiol. Immunol.* **41**, 527–535.
- Miyamoto, O., Minami, J., Toyoshima, T., Nakamura, T., Masada, T., Nagao, S., Negi, T., Itano, T., and Okabe, A. (1998). Neurotoxicity of Clostridium perfringens epsilon-toxin for the rat hippocampus via the glutamatergic system. *Infect. Immun.* **66**, 2501–2508.
- Miyata, S., Matsushita, O., Minami, J., Katayama, S., Shimamoto, S., and Okabe, A. (2001). Cleavage of a C-terminal peptide is essential for heptamerization of Clostridium perfringens epsilon-toxin in the synaptosomal membrane. *J. Biol. Chem.* **276**, 13778–13783.
- Miyata, S., Minami, J., Tamai, E., Matsushita, O., Shimamoto, S., and Okabe, A. (2002). Clostridium perfringens epsilon-toxin forms a heptameric pore within the detergent-insoluble microdomains of Madin-Darby canine kidney cells and rat synaptosomes. *J. Biol. Chem.* **277**, 39463–39468.
- Morgan, K.T., Kelly, B.G., and Buxton, D. (1975). Vascular leakage produced in the brains of mice by Clostridium welchii type D toxin. *J. Comp. Pathol.* **85**, 461–466.
- Morinaga, G., Nakamura, T., Yoshizawa, J., and Nishida, S. (1965). Isolation of Clostridium perfringens Type D from a case of gas gangrene. *J. Bacteriol.* **90**, 826.
- Mostowy, S., Boucontet, L., Mazon Moya, M.J., Sirianni, A., Boudinot, P., Hollinshead, M., Cossart, P., Herbomel, P., Levraud, J.P., and Colucci-Guyon, E. (2013). The zebrafish as a new model for the in vivo study of Shigella flexneri interaction with phagocytes and bacterial autophagy. *PLoS Pathog.* **9**, e1003588.
- Murrell, T.G., O'Donoghue, P.J., and Ellis, T. (1986). A review of the sheep-multiple sclerosis connection. *Med. Hypotheses* **19**, 27–39.
- Nagahama, M., and Sakurai, J. (1991). Distribution of labeled Clostridium perfringens epsilon toxin in mice. *Toxicol.* **29**, 211–217.
- Nagahama, M., and Sakurai, J. (1992). High-affinity binding of Clostridium perfringens epsilon-toxin to rat brain. *Infect. Immun.* **60**, 1237–1240.
- Nakajima, H., Yamamoto, K., Agarwala, S., Terai, K., Fukui, H., Fukuhara, S., Ando, K., Miyazaki, T., Yokota, Y., Schmelzer, E., et al. (2017). Flow-dependent endothelial YAP regulation contributes to vessel maintenance. *Dev. Cell* **40**, 523–536.e6.
- Oyston, P.C., Payne, D.W., Havard, H.L., Williamson, E.D., and Titball, R.W. (1998). Production of a non-toxic site-directed mutant of Clostridium perfringens epsilon-toxin which

- induces protective immunity in mice. *Microbiology* 144 (Pt 2), 333–341.
- Parg, C., Seng, W.L., Semino, C., and McGrath, P. (2002). Zebrafish: a preclinical model for drug screening. *Assay Drug Dev. Technol.* 1, 41–48.
- Petit, L., Gibert, M., Gillet, D., Laurent-Winter, C., Boquet, P., and Popoff, M.R. (1997). Clostridium perfringens epsilon-toxin acts on MDCK cells by forming a large membrane complex. *J. Bacteriol.* 179, 6480–6487.
- Petit, L., Gibert, M., Gouch, A., Bens, M., Vandewalle, A., and Popoff, M.R. (2003). Clostridium perfringens epsilon toxin rapidly decreases membrane barrier permeability of polarized MDCK cells. *Cell Microbiol.* 5, 155–164.
- Popoff, M.R. (2011). Epsilon toxin: a fascinating pore-forming toxin. *FEBS J.* 278, 4602–4615.
- Preston, M.A., and Macklin, W.B. (2015). Zebrafish as a model to investigate CNS myelination. *Glia* 63, 177–193.
- Radaram, B., Ivie, J.A., Singh, W.M., Grudzien, R.M., Reibenspies, J.H., Webster, C.E., and Zhao, X. (2011). Water oxidation by mononuclear ruthenium complexes with TPA-based ligands. *Inorg. Chem.* 50, 10564–10571.
- Ramnarayanan, S.P., and Tuma, P.L. (2011). MAL, but not MAL2, expression promotes the formation of cholesterol-dependent membrane domains that recruit apical proteins. *Biochem. J.* 439, 497–504.
- Robertson, S.L., Li, J., Uzal, F.A., and McClane, B.A. (2011). Evidence for a prepore stage in the action of Clostridium perfringens epsilon toxin. *PLoS One* 6, e22053.
- Rumah, K.R., Linden, J., Fischetti, V.A., and Vartanian, T. (2013). Isolation of Clostridium perfringens type B in an individual at first clinical presentation of multiple sclerosis provides clues for environmental triggers of the disease. *PLoS One* 8, e76359.
- Rumah, K.R., Ma, Y., Linden, J.R., Oo, M.L., Anrather, J., Schaeren-Wiemers, N., Alonso, M.A., Fischetti, V.A., McClain, M.S., and Vartanian, T. (2015). The myelin and lymphocyte protein MAL is required for binding and activity of Clostridium perfringens epsilon-toxin. *PLoS Pathog.* 11, e1004896.
- Rumah, K.R., Vartanian, T.K., and Fischetti, V.A. (2017). Oral multiple sclerosis drugs inhibit the in vitro growth of epsilon toxin producing gut bacterium, Clostridium perfringens. *Front. Cell Infect. Microbiol.* 7, 11.
- Sakurai, J., Nagahama, M., and Fujii, Y. (1983). Effect of Clostridium perfringens epsilon toxin on the cardiovascular system of rats. *Infect. Immun.* 42, 1183–1186.
- Schaeren-Wiemers, N., Bonnet, A., Erb, M., Erne, B., Bartsch, U., Kern, F., Mantei, N., Sherman, D., and Suter, U. (2004). The raft-associated protein MAL is required for maintenance of proper axon-glia interactions in the central nervous system. *J. Cell Biol.* 166, 731–742.
- Schaeren-Wiemers, N., Valenzuela, D.M., Frank, M., and Schwab, M.E. (1995). Characterization of a rat gene, rMAL, encoding a protein with four hydrophobic domains in central and peripheral myelin. *J. Neurosci.* 15, 5753–5764.
- Serbedzija, G.N., Flynn, E., and Willett, C.E. (1999). Zebrafish angiogenesis: a new model for drug screening. *Angiogenesis* 3, 353–359.
- Shortt, S.J., Titball, R.W., and Lindsay, C.D. (2000). An assessment of the in vitro toxicology of Clostridium perfringens type D epsilon-toxin in human and animal cells. *Hum. Exp. Toxicol.* 19, 108–116.
- Soler-Jover, A., Dorca, J., Popoff, M.R., Gibert, M., Saura, J., Tusell, J.M., Serratos, J., Blasi, J., and Martin-Satue, M. (2007). Distribution of Clostridium perfringens epsilon toxin in the brains of acutely intoxicated mice and its effect upon glial cells. *Toxicon* 50, 530–540.
- Takaki, K., Davis, J.M., Winglee, K., and Ramakrishnan, L. (2013). Evaluation of the pathogenesis and treatment of Mycobacterium marinum infection in zebrafish. *Nat. Protoc.* 8, 1114–1124.
- Tam, S.J., Richmond, D.L., Kaminker, J.S., Modrusan, Z., Martin-McNulty, B., Cao, T.C., Weimer, R.M., Carano, R.A., van Bruggen, N., and Watts, R.J. (2012). Death receptors DR6 and TROY regulate brain vascular development. *Dev. Cell* 22, 403–417.
- Tamai, E., Ishida, T., Miyata, S., Matsushita, O., Suda, H., Kobayashi, S., Sonobe, H., and Okabe, A. (2003). Accumulation of Clostridium perfringens epsilon-toxin in the mouse kidney and its possible biological significance. *Infect. Immun.* 71, 5371–5375.
- Taylor, K.L., Grant, N.J., Temperley, N.D., and Patton, E.E. (2010). Small molecule screening in zebrafish: an in vivo approach to identifying new chemical tools and drug leads. *Cell Commun. Signal.* 8, 11.
- Urich, E., Lasic, S.E., Molnos, J., Wells, I., and Freskgard, P.O. (2012). Transcriptional profiling of human brain endothelial cells reveals key properties crucial for predictive in vitro blood-brain barrier models. *PLoS One* 7, e38149.
- Uzal, F.A. (2004). Diagnosis of Clostridium perfringens intestinal infections in sheep and goats. *Anaerobe* 10, 135–143.
- Uzal, F.A., Kelly, W.R., Morris, W.E., and Assis, R.A. (2002). Effects of intravenous injection of Clostridium perfringens type D epsilon toxin in calves. *J. Comp. Pathol.* 126, 71–75.
- Uzal, F.A., Kelly, W.R., Morris, W.E., Bermudez, J., and Baison, M. (2004). The pathology of peracute experimental Clostridium perfringens type D enterotoxemia in sheep. *J. Vet. Diagn. Invest.* 16, 403–411.
- Wagley, S., Bokori-Brown, M., Morcrette, H., Malaspina, A., D'Arcy, C., Gnanapavan, S., Lewis, N., Popoff, M.R., Raciborska, D., Nicholas, R., et al. (2018). Evidence of Clostridium perfringens epsilon toxin associated with multiple sclerosis. *Mult. Scler.* 25, 653–660.
- Worthington, R.W., and Mulders, M.S. (1975). Effect of Clostridium perfringens epsilon toxin on the blood brain barrier of mice. *Onderstepoort J. Vet. Res.* 42, 25–27.
- Xie, J., Farage, E., Sugimoto, M., and Anand-Apte, B. (2010). A novel transgenic zebrafish model for blood-brain and blood-retinal barrier development. *BMC Dev. Biol.* 10, 76.
- Zhang, J., Ni, C., Yang, Z., Piontek, A., Chen, H., Wang, S., Fan, Y., Qin, Z., and Piontek, J. (2015). Specific binding of Clostridium perfringens enterotoxin fragment to Claudin-b and modulation of zebrafish epidermal barrier. *Exp. Dermatol.* 24, 605–610.
- Zhang, Y., Chen, K., Sloan, S.A., Bennett, M.L., Scholze, A.R., O'Keeffe, S., Phatnani, H.P., Guarnieri, P., Caneda, C., Ruderisch, N., et al. (2014). An RNA-sequencing transcriptome and splicing database of glia, neurons, and vascular cells of the cerebral cortex. *J. Neurosci.* 34, 11929–11947.
- Zhou, G., Liang, F.X., Romih, R., Wang, Z., Liao, Y., Ghiso, J., Luque-Garcia, J.L., Neubert, T.A., Kreibich, G., Alonso, M.A., et al. (2012). MAL facilitates the incorporation of exocytic uroplakin-delivering vesicles into the apical membrane of urothelial umbrella cells. *Mol. Biol. Cell* 23, 1354–1366.
- Zhu, C., Ghabriel, M.N., Blumbergs, P.C., Reilly, P.L., Manavis, J., Youssef, J., Hatami, S., and Finnie, J.W. (2001). Clostridium perfringens prototoxin-induced alteration of endothelial barrier antigen (EBA) immunoreactivity at the blood-brain barrier (BBB). *Exp. Neurol.* 169, 72–82.

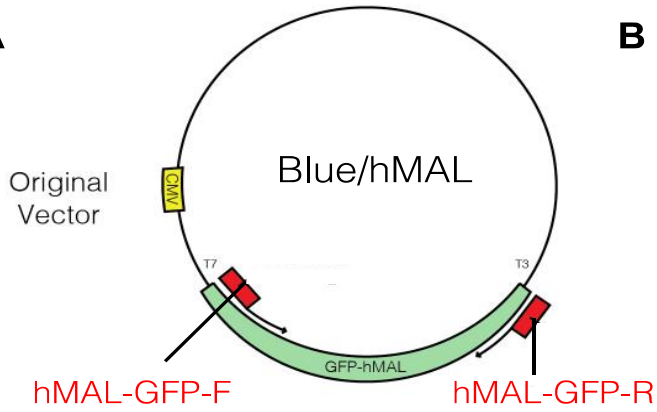
ISCI, Volume 15

Supplemental Information

***Clostridium perfringens* Epsilon Toxin Compromises the Blood-Brain Barrier in a Humanized Zebrafish Model**

Drew Adler, Jennifer R. Linden, Samantha V. Shetty, Yinghua Ma, Monika Bokori-Brown, Richard W. Titball, and Timothy Vartanian

SUPPLEMENTAL FIGURE TITLES AND LEGENDS

A**B**

TYPE OF GENE	PRIMER	Melting Temp (°C)
hMAL/hBENE/ GFP-F	5'CACCATGGTGA GCAAGGGCG3'	73
hMAL-GFP-R	5'TTATGAAGACT TCCATCTGA3'	55
hBENE-GFP-R	5'TCAGTGGTAAT AGATGCTG3'	53

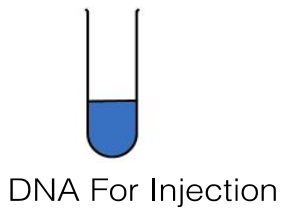
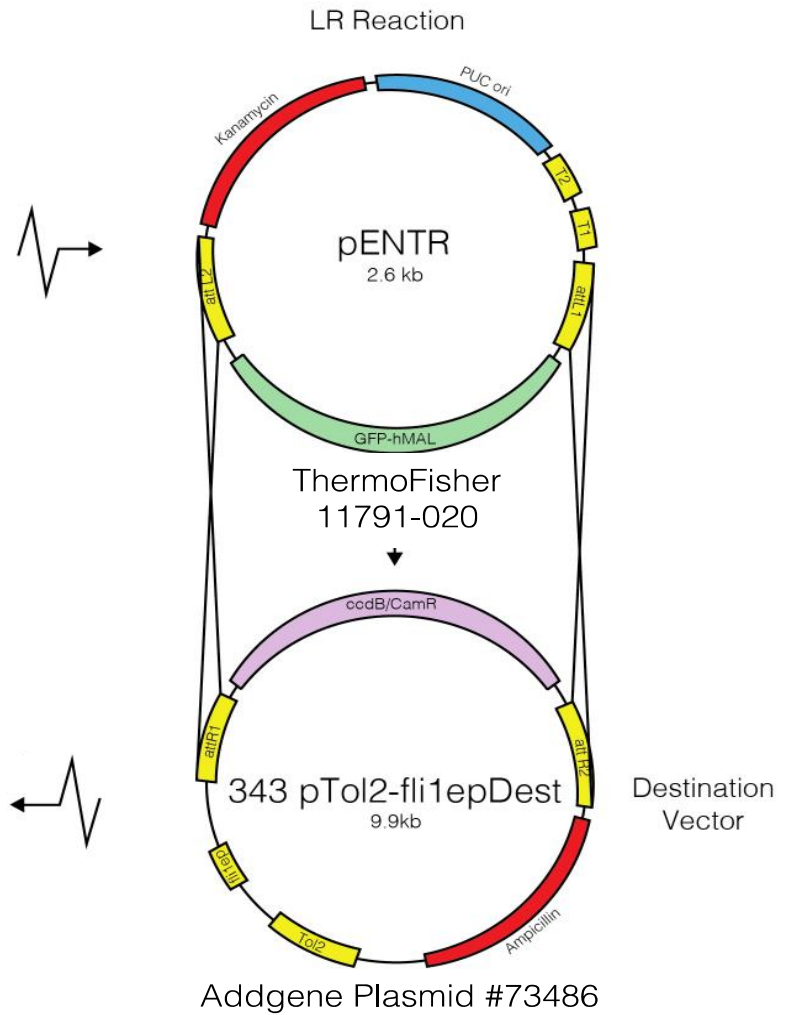
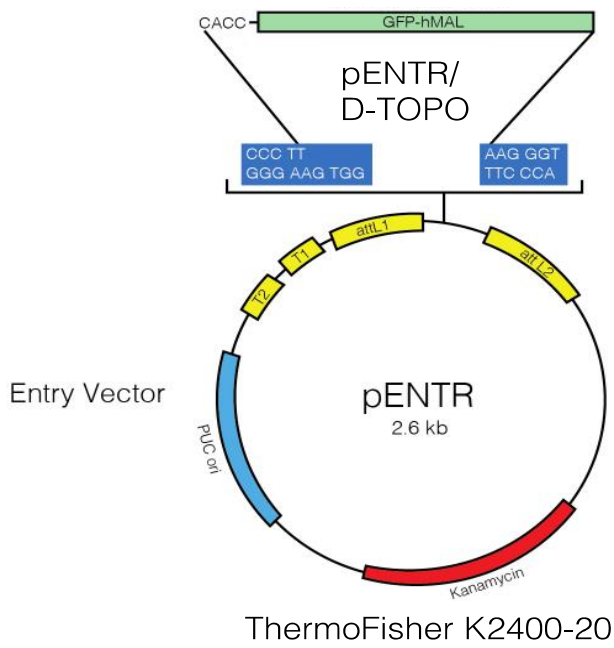


Figure S1. Overview of Gateway cloning strategy used to move hMAL-GFP and hBENE-GFP to the zebrafish endothelial specific vector (fli1 promoter/enhancer). Related to Figures 2, 3, and 4.

(A) Primers were generated (B) to excise hMAL-GFP from the “Original Vector” with extra 5’ CACC on the forward primer using blunt end PCR. PCR product reacted with and recombined into “pENTR/D-TOPO” plasmid to generate an “Entry Vector.” Entry vector reacted with “Destination Vector” containing fli1 enhancer/promoter using clonase II enzyme in a subcloning step known as the “LR Reaction”. This step uses clonase II enzyme which exchanges functional gene flanked by attL1/attL2 with toxic gene “cccB” flanked by attR1/attR2 sites. Only bacteria with correctly reacted plasmid survive (others are killed by unremoved toxic gene cccB). The final plasmid is then referred to as the “Final Expression Vector” and contains the functional, GFP-tagged gene flanked by attB1/attB2 sites, endothelial promoter, and Tol2 transposes recognition sites. Each plasmid step is amplified in chemically competent bacteria, plated on antibiotic selective agar, and isolated using miniprep.

hMAL-GFP + Neutralized ETX

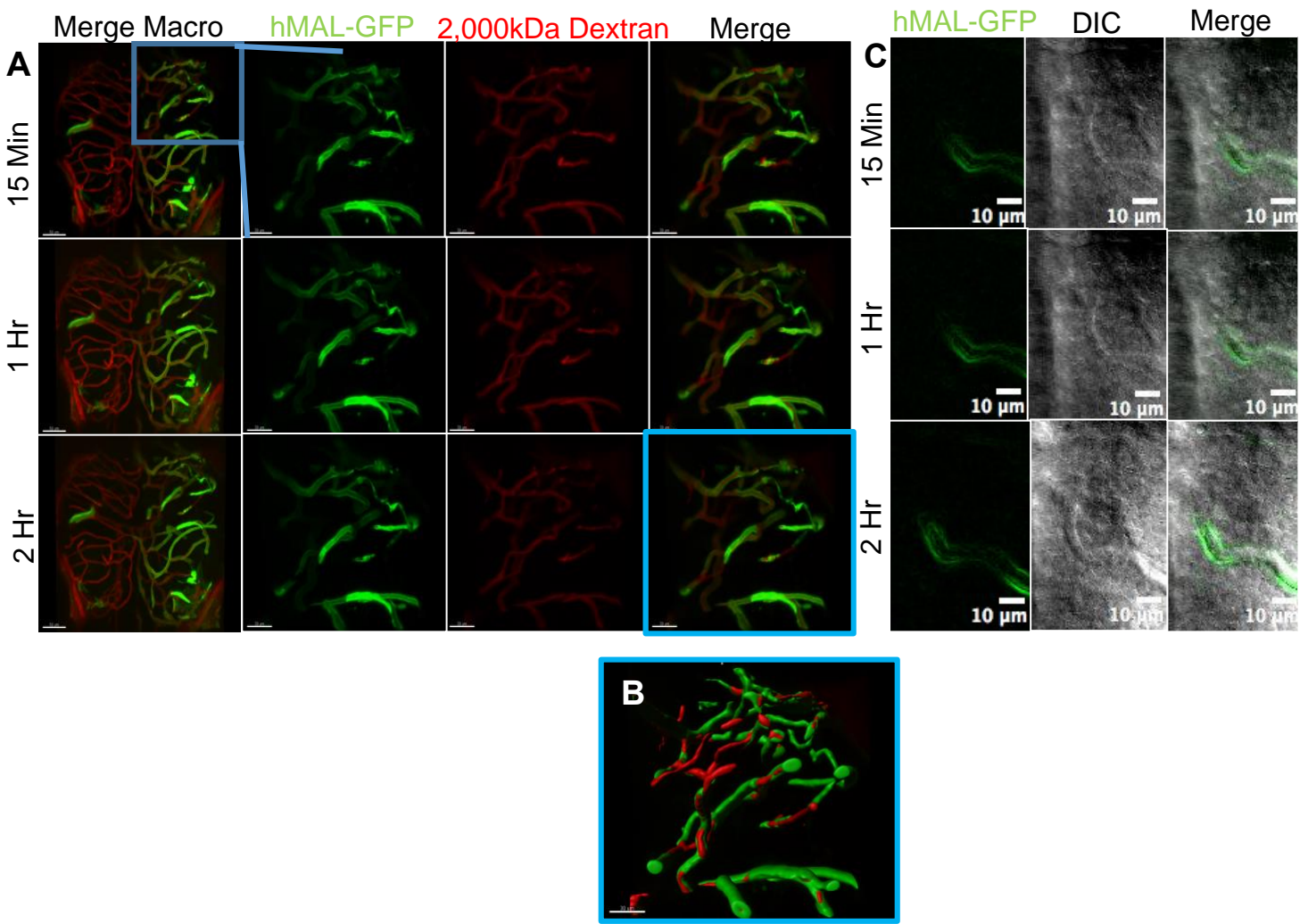


Fig S2. ETX antibody neutralization eliminates dextran leakage and vascular pathology in hMAL-GFP expressing fish. Related to Figure 7.

(A) 40X confocal images of hMAL-GFP expressing neurovasculature (green) co-injected with 2,000 kDa Dextran (red) and neutralized ETX at 15MPI, 1 HPI, and 2HPI. First three columns represent 3-D volumes depicted in “Merge Macro” blue box. Scale bars= 30 μ m in first three columns and 50 μ m in “Merge Macro” column. (B) Example of 2HPI Imaris 3-d rendering of hMAL-GFP and Dextran surfaces. (C) hMAL-GFP expression and DIC confocal imaging of CCTA vessel at the three time points.

hMAL-GFP + H149A pETX

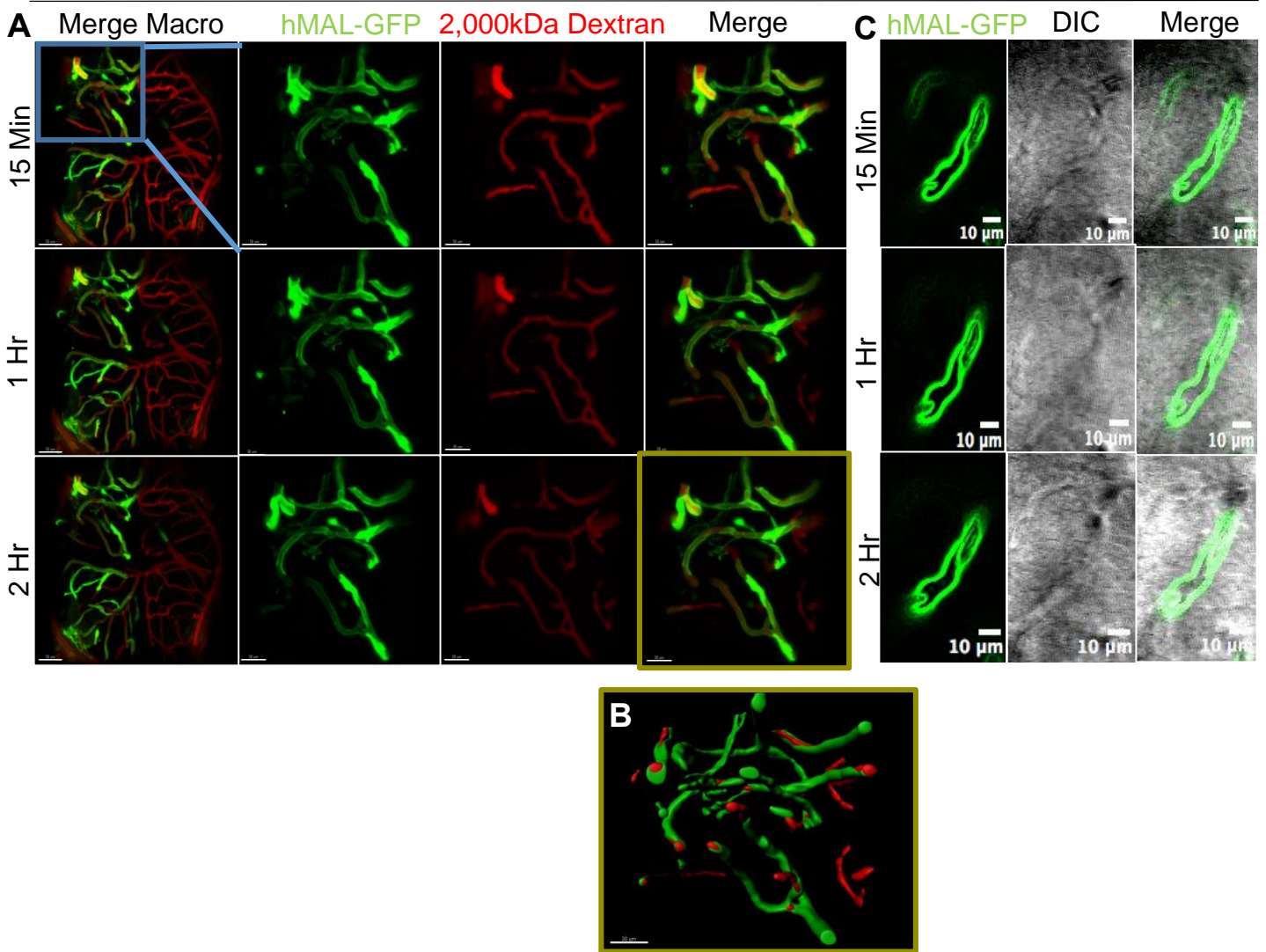


Fig S3. H149A mutant pETX fails to elicit dextran leakage or vascular pathology in hMAL-GFP expressing fish. Related to Figures 3 and 5.

(A) 40X confocal images of hMAL-GFP expressing neurovasculature (green) co-injected with 2,000 kDa Dextran (red) and H149A pETX at 15MPI, 1 HPI, and 2HPI. First three columns represent 3-D volumes depicted in “Merge Macro” blue box. Scale bars= 30µm in first three columns and 50µm in “Merge Macro” column. **(B)** Example of 2HPI Imaris 3-D rendering of hMAL-GFP and Dextran surfaces. **(C)** hMAL-GFP expression and DIC confocal imaging of CCTA vessel at the three time points.

Movie S4. Alexa-tagged pETX has affinity for hMAL-GFP ISVs. Related to Figure 2.

A representative time-lapse video of tagged pETX accumulating at the edge of an hMAL-GFP vessel. The first half of the movie just shows the red pETX channel. While the second half is a repeat with both the red pETX channel and the green hMAL channel.

Movie S5 Alexa-tagged pETX has no affinity for hBENE-GFP ISVs. Related to Figure 2.

A representative time-lapse video of tagged pETX failing to accumulate at a hBENE-GFP vessel. The first half of the movie just shows the red pETX channel. While the second half is a repeat with both the red pETX channel and the green hBENE channel.

Movie S6. Alexa-tagged H149A mutant pETX shows subtle affinity for hMAL-GFP ISVs. Related to Figure 2.

A representative time-lapse video of tagged pETX accumulating at the edge of an hMAL-GFP vessel. The first half of the movie just shows the red pETX channel. While the second half is a repeat with both the red H149A mutant pETX channel and the green hMAL channel.

Movie S7. ETX causes stark leakage in hMAL-GFP neurovasculature. Related to Figures 3 and 4.

A representative confocal Z-Stack traversing ventrally through the neurovasculature of a hMAL-GFP expressing fish. All evident leakage appears adjacent to hMAL-GFP vessels. The red channel represents 2.000 kDa Rhodamine Dextran. The green channel represents hMAL-GFP. The grey background is DIC imaging.

Movie S8. ETX causes no leakage in hBENE-GFP neurovasculature. Related to Figure 3.

A representative confocal Z-Stack traversing ventrally through the neurovasculature of a hBENE-GFP expressing fish. All red dextran appears confined in blood vessels. The red channel represents 2.000 kDa rhodamine dextran. The green channel represents hBENE-GFP. The grey background is DIC imaging.

Movie S9. ETX causes perivascular edema in hMAL-GFP neurovessels. Related to Figure 5 and S7.

A representative Z-Stack using the DIC channel (Same stack as Movie S7) reveals edema in select hMAL expressing blood vessels. The red arrow highlights edema.

Movie S10. ETX causes no perivascular edema in hBENE-GFP neurovessels. Related to Figure 5 and S8.

A representative Z-Stack using the DIC channel (Same stack as Movie s8) reveals no edema in any hBENE expressing blood vessels.

Movie S11. ETX terminates blood flow in hMAL-GFP neurovessels. Related to Figure 5.

A representative comparison of blood vessels at the midline the brain of an hMAL-GFP fish evidences continued blood-flow in a blood vessel without recognizable hMAL-GFP expression and stopped blood-flow in an hMAL GFP Vessel after injection of ETX. Red represents 2,000 kDa rhodamine dextran. Green represents hMAL-GFP. The grey background is DIC imaging. Movie taken at 50 MPI.

Movie S12. ETX fails to terminate blood flow in hBENE-GFP neurovessels. Related to Figure 5.

A representative comparison of blood vessels at the midline the brain of an hBENE-GFP fish evidences blood-flow in both a blood vessel without recognizable hBENE-GFP expression and in an hBENE-GFP Vessel after injection of ETX. Red represents 2,000 kDa rhodamine dextran. Green represents hBENE-GFP. The grey background is DIC imaging. Movie taken at 50MPI.

Movie S13. H149A mutant pETX fails to terminate blood flow in hMAL-GFP neurovessels.

Related to Figure S3.

A representative comparison of blood vessels at the midline the brain of an hMAL-GFP fish evidences blood-flow in both a blood vessel without recognizable hMAL-GFP expression and in an hMAL-GFP Vessel after injection of H149A pETX. Red represents 2,000 kDa rhodamine dextran. Green represents hMAL-GFP. The grey background is DIC imaging. Movie taken at 50MPI.

Movie S14. Antibody neutralization of ETX restores blood flow in hMAL-GFP neurovessels.

Related to Figure S2.

A representative comparison of blood vessels at the midline the brain of an hMAL-GFP fish evidences blood-flow in both a blood vessel without recognizable hMAL-GFP expression and in an hMAL-GFP Vessel after injection of antibody neutralized ETX. Red represents 2,000 kDa rhodamine dextran. Green represents hMAL-GFP. The grey background is DIC imaging. Movie taken at 50 MPI.

TRANSPARENT MATERIALS AND METHODS

Ethics Statement

All procedures conform to the National Institutes of Health guidelines regarding animal experimentation and were approved by Cornell University's Institutional Animal Care and Use Committees.

Genetic Cloning into Endothelial Specific Vector

Plasmids containing GFP fused to Human Myelin and Lymphocyte protein (hMAL-GFP) or the Human Myelin and Lymphocyte Like protein (hMALL or hBENE-GFP) were donated by the Vartanian Lab in a pBluescript II KS +/- vector initially under a CMV promoter. Both fusion genes were blunt end PCR amplified with Phusion High-Fidelity Polymerase (NEB) and primers were generated (Thermo Fisher) for cloning (Fig. S1b). PCR products were then gel purified using a gel purification kit (Qiagen) and cloned into a pENTR Directional TOPO vector (Thermo Fisher) for Gateway cloning as per manufacturer's instructions. The plasmid mixture was then amplified in One Shot Top Ten chemically competent *Escherichia coli* (Thermo Fisher), plated on selective agar, isolated with mini prep (Qiagen), and sequenced (Genewiz). Overlapping sequences were aligned using SeqManPro (DNASTAR) and compared to Pubmed reference sequence (hMAL Gene ID: 4118, hBENE Gene ID: 7851). Afterwards, sequence verification entry vectors containing both fusion genes were reacted with zebrafish endothelial specific enhancer/promoter *fli1* containing destination vector with Tol2, ccdB, and attR1/R2, sites: pTol2-fli1epDest was a gift from Nathan Lawson (Addgene plasmid # 73486). The reaction mixture was again used to transform One Shot Top Ten chemically competent *Escherichia coli*, which were plated on selective Ampicillin agar plates, clones expanded in liquid culture, plasmids isolated using mini prep, and sequenced for verification of correct final destination vector. A second control vector, GFP under the same enhancer/promoter (pTol2-fli1ep:EGFPDest), was delivered in a bacterial stab, a gift from Nathan Lawson (Addgene Plasmid #73491), streaked on a ampicillin selective agar, and isolated using mini prep. Tol2 transposase mRNA was generated from

the pT3TS-Tol2 plasmid that contained Tol2 transposase RNA under a T3 promoter. pT3TS-Tol2 was a gift from Stephen Ekker (Addgene plasmid # 31831) and was delivered in a bacterial stab, streaked on Ampicillin selective agar, and isolated using mini prep. Isolated DNA was transcribed to RNA *in vitro* using the mMESSAGE mMACHINE T3 transcription kit (Thermo Fisher), verified to contain a 2kb band using gel electrophoresis, and immediately stored at -80°C (See Fig. S1a).

Animal Husbandry

All experiments were performed on 1 to 8-day(s) post fertilization *casper* (*roy*; *nacre*) transgenic *Danio reiro* (zebrafish) (White et al., 2008). Fish were bred and maintained in the Fetcho fish facility at 28.5°C (Aquatic Ecosystems, Inc.). All experiments were performed at room temperature (~22-26°C). The remnants of the yolk sack provided sustenance for the entirety of experimentation.

Evaluation of toxin binding to MAL-expressing CHO cells

Chinese Hamster Ovary (CHO) cells expressing green fluorescent protein (CHO-GFP), GFP-rat MAL fusion protein (CHO^{GFP-rMAL}), or GFP-human MAL fusion protein (CHO^{GFP-hMAL}) were grown on a 12-well plate (Costar) until confluence was reached. Cells were washed and were either administered 0nM toxin, 50nM Titball et al. mutant H149A-pETX, or 50nM pETX for 1 hour at 37C. To transfer cells from 12-well plate into a 96-well plate (Corning), cells were trypsinized using 0.25% Trypsin-0.53 mM EDTA solution and added to an equal volume of Fetal Bovine Serum (FBS). Cells were then spun at 450 rcf for 5 minutes and re-suspended in PBS. In the 96 well plate, cells were stained with BD Horizon™ Fixable Viability Stain 450 (BD 562247) and fixed using Fixation Buffer (Biolegend 420801). Cells were then blocked and permeabilized using a solution consisting of 1X Intracellular Staining Permeabilization Wash Buffer (Biolegend 421002) + 10% Normal Donkey Serum (Jackson ImmunoResearch 017-000-121). ETX binding was assessed using an affinity

purified, rabbit polyclonal anti-ETX antibody (Rb204) for 20 minutes at room temperature. Normal Rabbit Serum Control (0.5ug/ml; Thermo Fisher Scientific 08-6199) was used as a negative control. Probed cells were washed using PBS + 2% FBS and antibody binding was detected using a PE-conjugated Donkey anti-Rabbit antibody (Biolegend 406421). Results were collected from treatment conditions performed in triplicate.

Injection and Transient Expression of Fusion Proteins in EC

hMAL-GFP/hBENE-GFP plasmids and Tol2 mRNA were diluted to 25 ng/μl in nuclease free water while the plasmid containing DNA (either hMAL-GFP or hBENE-GFP) and RNA (tol2 transposase) were mixed for co-injection into fertilized *casper* zebrafish eggs at the single cell stage. Glass microinjection needles were pulled using the P-97 Flaming/Brown Micropipette Puller (Sutter Instrument, Novato, CA) and were cut under a microscope with a single edged blade to a diameter ~1 micron. Needles were then filled with DNA/RNA mixtures and inserted in a micromanipulator (Narishige, USA) attached to the PLI-100 pico-injector (Harvard Apparatus, Holliston, MA) for consistent picolitre injections. Injection time and pressure were adjusted such that consistent injection volumes appeared 3 times the diameter of the needle tip. After barriers separating male and female adults were removed, eggs were collected and spread on a molded agarose plate with depressions such that the cell faced the needle. DNA/RNA mixtures were then injected into eggs and incubated at 28°C for 3 days. Egg injection was visualized using a Zeiss Stemi 2000 stereomicroscope. After incubation time, hatched larval zebrafish were screened for vascular specific GFP expression using a Leica M205 FA Fluorescence Stereo Microscope. GFP-positive fish were separated for toxin injections.

pETX Injections for Binding Assay

pETX (BEI Resources NR-856) was conjugated to Alexa Fluor 647 dye (Thermo Fisher A30009) and stored in glycerol at -20°C. H149A mutant pETX was provided by the Titball lab and a portion was conjugated to Alexa Fluor 647 dye (Thermo Fisher). The protoxin and mutant protoxin were diluted to 150ng/μl in .05% Bromthymol Blue, which was used for injection visualization, and pipetted into a pulled microinjection needle. Positive fish were anesthetized in .02% MS-222 (tricane) in 10% Hank's Balanced Salt Solution (HBSS) for one minute and then placed on a bed of agar under a chemical hood. Fish were oriented on their rostral sides with their heads facing away from the microinjection needle and the micromanipulator were angled at 45 degrees from its stand. Injection pressure was manipulated such that consistent volumes were emitted from the needle around 3 times the diameter of the 1 μm tip. The needle was slowly lowered until contact was made with the skin of the fish directly above the Duct of Cuvier. The manipulator was fidgeted such that the needle slowly penetrated skin and entered the duct. Four to six pulses were injected into the duct for systemic infection (Benard et al., 2012). Immediately after the last injection occurred, a stopwatch was started to mark t=0 for the binding assay.

Active ETX injections for BBB Permeability Assay

Six to seven DPF fish showing consistent transgene expression in the brain were isolated for active ETX injection or mutant H149A pETX. Fish were anesthetized in MS-222 as described above and placed on a petri dish with agarose. Toxins were diluted to a concentration of 150 ng/μl in 25% 2,000 kDa Tetramethylrhodamine Dextran (Thermo Fisher) (diluted to a final concentration of 4mg/ml) and filled a pre-cut pulled needle as described above. Toxin was injected into the Duct of Cuvier for systemic infection as described above. A timer commenced at the injection time and fish were quickly embedded in 1.42% LAMP agarose for confocal microscopy. BSL2 safety precautions were

maintained throughout injection set up and cleanup. All surfaces were bleached post injection and any disposable materials in contact with the toxin were autoclaved.

Active ETX Antibody Neutralization

Active ETX at a concentration of .321mg/ml was diluted 2:1 in JL008 (anti-ETX rabbit monoclonal antibody generated by the Vartanian Lab) and incubated in a polypropylene microfuge tube for 1hr at RT. The toxin/antibody mixture was then diluted in 2,000 kDa Tetramethylrhodamine dextran (Thermo Fisher, USA) such that the final concentration of toxin remained at 150 ng/ μ l and the final concentration of dextran was 4mg/ml prior to injection as described above.

In-vivo Confocal Microscopy

For Binding Experiments

Post Injection zebrafish were quickly moved from the injection agar to a dish with .02% MS-222. Zebrafish were transferred to a glass bottom dish with a central impression under a Zeiss Stemi 2000 stereomicroscope and extra fluid was aspirated away such that fish had minimal surrounding them. The viability of post injection fish was verified, and imaging was begun only if blood circulation remained constant as could be visualized under the microscope. Any fish with stopped or slowed blood flow, even if heartbeat persisted, were euthanized. Healthy fish were submerged in pre-melted 1.2% agar in 10% HBSS such that the entirety of the central depression was covered. Fish were pushed to the bottom of the depression with a tungsten wire and oriented with their dorsal sides down. After the agar solidified, a few drops of anesthetic were dripped on the agar to avoid desiccation and to prevent mortality throughout the imaging period. Fish were then scanned under a Zeiss 510 Inverted Confocal Microscope until a bright green intersegmental blood vessel (ISV) was found. Z-stack Time Lapse Imaging commenced as soon as such a vessel was located for a duration

of ~90minutes. The time of the first picture was referenced to the injection start stopwatch. Two separate channels were used to sense excitation by the multi-line Argon laser (488nm excitation for GFP) and the HeNe 633nm (for Alexa Fluor 647 excitation). The “switch track every line” option was chosen using the Zen 2009 imaging software (Zeiss, USA) for scans to minimize fluorescent bleed-over. Z-stacks were taken through the depth of the highlighted vessel every 30 seconds. Laser intensity was maintained at the same value for each fish.

For Toxicity Experiments

Post injection fish mounted in low melting point agarose as described above were positioned dorsal side. Fish were then moved to the Zeiss 510 confocal with 448 Argon laser and 543 HeNe on for GFP and rhodamine dextran imaging respectively and a DIC channel was used for tissue imaging. The fish were identified with the ocular setting using 40x magnification. The settings were switched to “acquisition mode” with zoom set to 0.7. Fish were assessed for noticeable dextran intensity in a consistent range flowing through blood vessels. Those with dim levels of dextran were eliminated from the study. If dextran intensity passed these criteria, fish were subjected to a full brain Z-stack at 15 min, 1 hr, and 2 hrs post injection. For each scan, orientation and depth were adjusted prior to capture to ensure scans included the same depth in each picture. A total of 115 Z-slices were taken per fish either through setting up a 115-slice z-stack or by cropping data post capture to equal 115 slices. Each fish was scanned through a depth of 115-120 μ l. At 50 min post injection, between the first and second z-stack, identical vessels on the left and right side of the brain, one which exhibited GFP expression and the other which did not, were imaged on a single plane at maximum speed for 3s to look for blood flow. Post-injected fish were euthanized.

Image Analysis

For Binding Analysis

Time-lapse Z-stack images were imported to Imaris 8.0.2 software (Bitplane) for image analysis. All images were registered to a green vessel at a time point midway through the time-lapse in three dimensions using an algorithm generated in MATLAB (MathWorks) to minimize the effects of plane drift. Equal areas along one side of the vessel were rendered into a 3D surface and within that surface the relative GFP and Alexa 647 intensity values were compared over the duration of imaging and averaged at each time point for each condition.

Colocalization analysis was conducted on the particular Z-stack at 60 min post injection. The image dataset was masked to the GFP channel such that only noticeable vessels, and not off-target expression, were included in analysis. After the data was masked, automatic threshold was performed on both channels using the Costes and Lockett algorithm to remove bias of visual interpretation. Within this threshold, the percent of Alexa-647 material above GFP threshold colocalized, was generated for each fish.

For Dextran Leakage Analysis:

Full brain z-stacks for each fish were imported to Imaris 8.0.2 software (Bitplane). Snapshots of the 3D images were taken with different filters using the “snapshot” function. For quantification of leakage, the image was cropped to a volume of 159x159x112 μm to include the area of the brain with the greatest degree of receptor expression. Within this area a baseline surface was generated out of the red channel using the identical inputs. The threshold of each individual surface was then toggled to only include continuous vesicular structures and any non-continuous structures still included were manually deleted. Leakage was quantified as the sum red (dextran) channel extravascular voxel intensities/intravascular voxel intensities (E/I). This ratio was garnered for each image using the equation:

Eq 1

$$\frac{E}{I} = \frac{SR_{total} - SR_{surface}}{SR_{surface}}$$

SR=sum intensity of red (dextran) voxels

Total=all voxels in the volume considered

Surface=voxels within the red surface

For Vessel Diameter Quantification:

Z-Stack Images were imported into ImageJ (NIH, USA) for image analysis. The Cerebellar Central Arteries (CCtAs) were identified for each fish, which had noticeable GFP expression. Only fish with noticeable GFP expression in at least one CCtA were considered. Edges on each image were clarified using the “Find Edges” function on ImageJ. Images were then zoomed in 300%, and an evaluator, blind to the experimental set up, measured the inner diameter of each vessel in three places along the process of the vessel, using the GFP channel. These three values were averaged for each vessel in each fish at each time point.

Activation of pETX to ETX

pETX in phosphate buffer (pH 7.4) at a concentration of .5mg/ml was thawed to room temperature. 25 µl of immobilized Trypsin TPCK treated (Thermo Fisher) was added to an eppendorf tube with 500µl of 10 mM sodium phosphate monohydrate buffer (pH 7.9). The resulting mixture was vortexed and spun three times on a tabletop centrifuge for 10 min and re-suspended in 200µl buffer. The protoxin was added, vortexed, and incubated in a shaking incubator at 37°C for 2 hrs after which it was isolated using top speed centrifugation for 10 min. Activated toxin was aliquoted and stored at -80°C until it was needed.

Ex Vivo Immunohistochemistry for Binding Assay

Seventeen-month-old adult *casper* zebrafish were anesthetized with 0.2% ms-222 and pinned on Styrofoam with tungsten wires. Whole brains were isolated from the fish and fixed in 4% PFA overnight. Brains were then suspended in 30% sucrose, for cyroprotection, at room temperature until they sunk to the bottom of a 50 mL conical tube. A metal beaker was filled with isopentane and placed on dry ice. Brains were placed in square molds, submerged in OCT solution (Sakura Finetek) and quickly frozen. Frozen tissue was then sliced into 12 μ M thick sections along the sagittal plane and adhered to gelatin coated slides.

C57BL/6 WT mice ages 8-16 weeks old were deeply anesthetized with CO₂, perfused with PBS via cardiac puncture, and euthanized with lethal doses of xylazine and ketamine. Brains were extracted and flash-frozen in OCT solution for cryosectioning. Sixteen-micron sagittal sections were cut and adhered to gelatin coated slides and stored at -20°C until used for immunohistochemistry.

Mouse tissue sections were fixed in 4% PFA for 10 min. Then both zebrafish and mouse tissue were blocked in PBS containing 10% goat serum, and .1% triton 100 for 30 minutes at room temperature in a humidity chamber. All tissue was then probed with pETX (.5mg/mL) 1:100 in blocking solution for 1 hr at room temperature in a humidity chamber. All sections were then washed in PBS 3 times for 5 min each and incubated in JL008 anti-ETX primary antibody (ATUM) at a 1:1000 in blocking solution for 1 hr at room temperature in a humidity chamber. A few zebrafish and mouse slides were left out of the primary staining step as controls. All sections then were washed 3 times in PBS as described above and exposed to Cy3 donkey anti-rabbit secondary at 1:500 (Jackson ImmunoResearch) and FITC Biotinylated Bandeiraea Simplicifolia Lectin 1 (BSL1), a family of glycoproteins which bind blood cells and can highlight vasculature, at 1:200 (Vector Labs) in blocking solution for 1 hr at room temperature in a humidity chamber. Sections were washed in PBS as described above and subsequently incubated in TrueBlack Lipofuscin (Biotium) for 30s to eliminate

autofluorescence. Sections were again washed 3x in PBS, mounted with DAPI (Vector Labs), and covered with 1.5 cover slips. Photos were taken with a SPOT cooled camera (Diagnostic Instruments) attached to Axioskop2 fluorescence microscope (Carl Zeiss). Photo exposure time was made constant for each condition to control discrepancies due to image capture. Images were imported to ImageJ64 (NIH) in 8-bit grey format for image processing.

Statistical Analysis

All statistical analyses and graph compositions were conducted using Prism version 7.00 for Mac (GraphPad Software). Student's T test, One Way ANOVA or Two Way ANOVA with Tukey's Post Hoc Test were used in analyses. $P < 0.05$ was considered significant. (* $P < 0.05$, ** $P < .01$, *** $P < .001$, **** $P < .0001$).

SUPPLEMENTAL REFERENCES

Benard, E.L., van der Sar, A.M., Ellett, F., Lieschke, G.J., Spaink, H.P., and Meijer, A.H. (2012). Infection of zebrafish embryos with intracellular bacterial pathogens. *J Vis Exp*.

White, R.M., Sessa, A., Burke, C., Bowman, T., LeBlanc, J., Ceol, C., Bourque, C., Dovey, M., Goessling, W., Burns, C.E., *et al.* (2008). Transparent adult zebrafish as a tool for in vivo transplantation analysis. *Cell Stem Cell* 2, 183-189.